J. Egypt. Acad. Soc. Environ. Develop., 21 (1):25-59 (2020) (D-Environmental Studies)
E.mail: easedjournal_egypt@yahoo.com ISSN 1110-8770
www.jades.journals.ekb.eg eISSN 2314-5471 (online)

Improvement and characterization of alum sludge by nano-iron oxide and rice husk for removal of methylene blue dye from aqueous solution

Tamer T. El-Tokhy[3], Mohamed A. Ahmed[1*], Maie I. ElGammal[2] and Mahmoud S. Ibrahim[2]

1*- Chemistry Department, Faculty of Science, Ain Shams University, Cairo, Egypt.
2- Environmental Science Department, Faculty of Science, Damietta University, Egypt.
3- Labs and Research Sector, Greater Cairo Drinking Water Company, Cairo, Egypt.

Received May 25, 2020
Accepted: August 30, 2020

ABSTRACT

In the present study, the adsorption characteristics of the alum sludge (AS) waste from Rod El-Farag water treatment plant was improved by treatment with acidic rice husk (RH) and Nano-Magnetite (N.M) to form Nano-Magnetite composite (ASRHNMC). This composite gained new characteristics of large surface area, mesoporous structure and magnetic properties and it was used as a low cost adsorbent for the removal of methylene blue (MB) as a cationic dye from aqueous solution. (AS) and (ASRHNMC) were characterized by FT-IR, XRD, BET N_2, EDX, SEM, TEM and XRF and were compared to adsorption ability against MB dye. The pH of the solution, sorbent dose, initial dye concentration, contact time and temperature were investigated using batch sorption technique for (MB) dye.

The experimental results have pointed out that the adsorption equilibrium data is fitted well to the Langmuir isotherm reflecting favor formation of monolayer of MB dye on composite surface. The value of enthalpy change indicating that the removal process is endothermic. The adsorption process follows pseudo-second order rate equation and the negative values of standard free energy (ΔG°) suggested that the adsorption process is spontaneous. The repeatability and regeneration studies of (ASRHNMC) for adsorption of MB were investigated and the results indicated the ability of reuse this composite several times in removal of MB from aqueous solutions.

Keywords: Alum sludge, recycling, adsorption, methylene blue, rice husk, Nano-Magnetite.

INTRODUCTION

Alum sludge is a by-product from the processing of drinking water in drinking water treatment plants. Alum sludge produced when alum (aluminium sulfate) is used as coagulant. The disposal of this sludge to a landfill causes environmental problems; since alum sludge contains a high level of aluminium, which has been shown to be toxic to aquatic life and relatively inert, providing marginal benefits to soil fertility. Moreover, the reuse of alum will be economically and environmentally beneficial (Raseid *et al.*, 2016). Previous studies have shown that drinking water treatment sludge (Alum sludge) can be used as an effective adsorbent for phosphate (Al-Fatlawi and Neamah, 2015), some heavy metals and dyes removal (Nasser *et al.*, 2017; Zhou e*t al.*, 2010; Lee *et al.*, 2006).

Rice husk is the outer covering of the rice grain, which is a by-product of the rice milling process. It is an agricultural waste material in all rice-producing countries. Most of the rice husk usually ends up either being dumped or burned in open spaces, thus causing damage to the land and environmental pollution. Many efforts have been made to utilize the rice husk including as an alternative fuel for energy production (Nasser *et al.*, 2017;

Chungsangunsit *et al.*, 2010). The major components of rice husk are organic materials such as hemicellulose, cellulose and lignin totaling about 75- 90% and the remaining ash content of 17-20% (Tribe, N., 1974). The ash mainly consists of >90% silica and some metallic impurities. Combustion of rice husk under controlled conditions leads to the productions of rice husk ash containing almost pure silica. The metallic impurities such as iron (Fe), manganese (Mn), calcium (Ca), sodium (Na), potassium (K) and magnesium (Mg) that influence the purity and color of the silica could be eliminated by pretreatments with hydrochloric acid, sulfuric acid or nitric acid prior to combustion (Yalcin and Sevinc, 2001).

Magnetic nanoparticles (MNPs) are a class of nanoparticles which can be manipulated using a magnetic field. MNPs have the advantages of large surface area, high number of surface active sites and high magnetic properties, which cause high adsorption efficiency, high removal rate of contaminants, easy and rapid separation of adsorbent from solution via magnetic field. After magnetic separation, the contaminants can be easily removed from nanoparticles by the desorbent agents, and the recovered MNPs can be reused (Zhang *et al.*, 2020; Besharati, N., *et al.*, 2018; Oliveira *et al.*, 2003).

Dyes and pigments are widely used in the textiles, paper, plastics, leather, food, and cosmetic industries for coloring products. Most of dyes are toxic and must be removed before discharge into receiving streams (Hashemian *et al.*, 2015). The discharge of effluents from these industries contain large amount of dyes, not only damage the aesthetic nature of receiving water bodies, but also may be toxic to aquatic life (Mohamed *et al.*, 2019).

Methylene blue (MB) dye belongs cationic dyes and has been reported to cause adverse health effects to humans, wildlife, and microorganisms and also to increase dangers in the environment by releasing toxic substances (Xiao *et al.*, 2015; Kuai and Nan, 2014; Alyoshina and Parfenyuk, 2013). In particular, in humans, MB can cause adverse health effects such as eye burns, cyanosis, methemoglobinemia, convulsions, tachycardia, dyspnea, and skin irritation. Thus, removal of methylene blue from wastewater is essential (Corda and Kini, 2018; Xiao *et al.*, 2015).

Numerous physicochemical treatment techniques, such as chemical oxidation (Salem and El-Maazawi, 2000), biodegradation (Jurado *et al*., 2006), ultrafiltration (Doke and Yadav, 2014), photodegradation (Kuo and Ho, 2001), extraction (Regel-Rosocka and Szymanowski, 2005), and adsorption (Fu *et al.*, 2011; Gong *et al.*, 2009), have been developed to treat MB. Among these methods, adsorption systems offer promising results for the removal of MB because they are simple, economical, and easy to operate

The present study is an attempt to explore the possibility to improve the adsorption characters of alum sludge from water treatment plant by rice husk as an agriculture waste and nano-magnetite to produce Nano-Magnetite Ternary Composite (Alum Sludge- Nano-Magnetite -Rice Husk) as a new effective costless adsorbent for the removal of water contamination caused by MB dye as a type of cationic dye.

MATERIALS AND METHODS

All chemical materials were purchased from Merck Company and used without any further purification, the Methylene Blue dye was purchased commercially from El-Gomhoria Company, Egypt.

1. Adsorbent:

1.1 Alum Sludge (AS)

It was obtained from Rod El-Farag water treatment plant in Cairo, Egypt. It was dried at 105^{o}C for 24 h till complete dryness, cooled to room temperature in desiccators, crushed and grinded till it became fine powder then it was sieved to 0.2 mm particle size (Raseid*et al.*, 2016)

Improvement and characterization of alum sludge by nano-iron oxide and rice husk for removal of methylene blue dye from aqueous solution.

1.2 Rice Husk (RH)

It was brought from Alsharqiea, Egypt, washed several times with tap water to remove adhering soil and clay, washed three times with deionized water, dried in oven at 60^0C till dryness then it was acid treated with 1M HCl in order to increase Amorphous silica content percentage of husk ash via; 10 g of washed and dried rice husk was soaked in a beaker containing 100 ml of 1M HCl and stirred for 2 hr (Maksum, A. *et al.,* 2017; Kurama and Kurama, 2003). It was washed by tap water several times and final wash with deionized water then it was dried at 60^0C till complete dryness.

1.3. Thermally Activation and improvement of Alum Sludge with Rice Husk.

Prepared alum sludge (AS) and acid treated rice husk (RH treated) were mixed with weight ratio of (2:1) rice husk to alum sludge then calcinated at 700^0C for 2hr by electric muffle furnace to improve the adsorption characteristics of (AS) (Nasser H. Shalaby *et al.,* 2017). The temperature (700^oC) was determined as optimum temperature in previous studies to obtain highly percentage of amorphous silica from (RH) for high adsorption (Maksum, 2017; Iara *et al.,* 2017; Rhaman *et al.,* 2015; Kurama and Kurama, 2003). Also, 700^oC for 2hrs has been chosen in the present study for calcination since the activated sludge adsorbents developed by physical activation at 700^oC from drinking water treatment (AS) are suitable adsorbents to remove metals and cationic dyes (Soleha *et al.,* 2017). The result powder was grinded and sieved to particle size between100 to 150 μm (Yusuff, 2017) and stored in polyethylene bottles with screwed caps. This composite was named by Alum Sludge Rice Husk Composite (ASRH).

1.4. Nano-magnetite preparation:

Fe_3O_4 nanoparticles were prepared by co-precipitation method. (0.1M) of ferrous sulfate ($FeSO4{\cdot}7H_2O$), (0.2M) of ferric chloride ($FeCl_3{\cdot}6H_2O$), 10% solution of Cetyl Trimethyl Ammonium Bromide (CTAB) and (2M) NaOH solution. 250 ml of (0.1M) ferrous sulfate was mixed vigorously with 250 ml of (0.2M) ferric chloride for about 30 min, 50 ml of 10% solution of Cetyl Trimethyl Ammonium Bromide was added and the solution and was stirred vigorously again for 2hrs at room temperature. NaOH (2M) solution was added drop by drop till black crystals were formed. The obtained Fe_3O_4 precipitant was separated with a magnet and was repeatedly washed with deionized water. The washed black precipitate was dried in oven at 50^0C for 4hrs (Fatemeh *et al.,* 2013). It was characterized by XRD, FT-IR, TEM and VSM. The chemical reaction of Fe_3O_4 precipitation is expected as follows:

$Fe^{+2} + 2Fe^{+3} + 8OH^- \rightarrow Fe_3O_4\downarrow + 4H_2O$

1.5. Preparation of Alum Sludge-Rice husk-Nano-magnetite ternary composite (ASRHNMC):

HCl (0.01M) and NaOH was prepared to adjust the pH to the target value. 0.14 g of Nano magnetite was grinded. 1g (ASRH) of composite. ASRHNMC was prepared with a weight ratio of Nano-Fe_3O_4 to (ASRH) (0.14:1) had the highest specific surface area and optimum, homogeneous pore volume for adsorption in addition to the magnetic character. If the ratio of nano-Fe_3O_4 increases higher than that ratio causes a decrease in the specific surface area and pore size of composite by the introduction of the nano-magnetite in the pore frameworks. If the of nano-Fe_3O_4 decreases lower than the ratio selected, the composite will lose its suitable magnetic character and optimum pore size volume for adsorption (Kittappa, S. *et al.,* 2015).

Two beakers each contains 25 ml of deionized water with pH 5.7 were prepared. One gram of (ASRH) composite was added in one beaker and 0.14 g of nano-magnetite was put in

the second one. Each solution was stirred with glass rod and the pH value readjusted again at 5.7. The 2 solutions were stirred again for 1 hr. then were mixed and stirred with glass rod for 2 hrs then remain without stirring for 24 hrs. The composite was separated with a magnet and was put in the oven at 100^{o}C for 1 hr. Finally the dried (ASRHNMC) composite was grinded.

2.Characterization and Morphological features of adsorbent:

2.1. Determination of point of zero charge (pH pzc)

The (ASRH) and (N.M) were measured. A standard solution of (0.1M) KNO_3 was prepared. A series of beakers was prepared each one contained 100 ml of (0.1M) KNO_3, the pH was adjusted in each beaker solution at a definite pH value (2, 3, 4, 5, 6, 7, 8, 9, 10, 11 and 12) by adding either (0.1 M) HCl or (0.1 M) NaOH, using pH meter. 0.1 g of sample was added in each beaker solution and the beakers were placed on shaker at 120 rpm and 25^{o}C for 24h. The pH measurement was repeated again after 24 hr for each solution. We plotted a relation curve between the initial pH ($pH_{initial}$) and pH after 24 hr (pH_{24hr}). Intersection point of the resulting curve with the line passing origin (pH_{24hr} =$pH_{initial}$) gives pH_{pzc} (Tauana *et al.*, 2019).

2.2. X-ray diffraction pattern (XRD)

The (AS), (ASRH), (N.M) and (ASRHNMC) powders were measured by X-ray diffractometer apparatus (Bruker, Darmstadt, Germany). X'PERT PRO MPD, with Cu Kα radiation (λ = 1.5406 A°). The scanning speed was 2◦/mm. The diffraction intensity curves with 2θ from 5 to 90◦ were obtained.

2.3. Fourier transform infrared spectrophotometer (FT-IR)

FTIR spectra were recorded for (AS), (ASRH), (N.M) and (ASRHNM) on BRUKER Tensor 37 Fourier transform infrared spectrophotometer, in the range from 400 – 4000 cm-1 using KBr pellets.

2.4. Energy dispersive X-Ray spectroscopy (EDX)

The elemental analysis of the dried raw Alum Sludge (AS), (ASRH) and the synthesized (ASRHNM) were done byEnergy Dispersive X-Ray spectroscopy (EDX), Ametek, U.S.A.

2.5. Scanning electron microscope (SEM)

Scanning Electron Microscope (SEM) analysis was done for (AS), (ASRH) and (ASRHNMC) using a scanning electron probe micro analyzer (JXA-840A, Japan). The specimen in the form of films were mounted on the specimen stabs and coated with thin film of gold by the sputtering method. The micrograph was taken at magnification of 500, 1000, and 2000 using (KV) accelerating voltage.

2.6. Transmission electron microscopy (TEM)

The TEM observation was carried out at 200kV acceleration voltages (Jeol–Jem 100cx Electron Microscope, Japan,). The (N.M) and (ASRHNMC) samples were carefully grounded, dispersed in acetone followed by sonication to get a solution of metal nanoparticles and placed on a micro grid using a drop of the dispersion. The sample chamber for the observation was kept cold using a liquid nitrogen bath to prevent the destruction of the sample by the high-voltage electron beam.

2.7. Brunauer, Emmett, and Teller Surface Area Analysis (BET)

BET surface area analyses were carried out for (AS), (ASRH), (N.M) and (ASRHNMC) samples using a Quantachrome Autosorb-1 Model ASIT adsorption apparatus. Adsorption isotherms were obtained under N2 at a temperature of 77K. The BET surface areas were calculated using the adsorption points at the relative pressures (P/Po) 0.05 - 0.25.

2.8. X-ray fluorescence (XRF) spectrometer

Chemical composition of (As), (As) after calcination at 700^{o}C (AS700), acid treated (RH) after calcination at 700^{o}C (RH700) and (ASRH) samples after were analyzed comparatively in an energy dispersive X-ray fluorescence (XRF) spectrometer (EDX 720 HS, Shimadzu). The results are expressed as percent by mass calculated over oxide content and normalized to 100% using carbon percent levels.

3. Optimization studies

The batch equilibrium technique was used to study the influence of various experimental controlling factors affecting the removal of methylene blue dye (MB) using (AS) and (ASRHNMC) including a comparative adsorption study and showing the adsorption behavior of (AS) and (ASRHNMC) with the same concentration to know the differences in the adsorption behavior of (AS) as an adsorbent before and after improvement. These included the effect of pH, contact time, sorbent dosage, adsorption capacity (initial adsorpate concentration) and (temperature and thermal adsorption studies) according to the following procedures.

3.1. Preparation of adsorbate (M.B dye)

MB dye used in this study was of commercial purity. A stock solution of MB (100 ppm) was prepared by dissolving the required quantity of the dye in deionized water. The working dye solution was prepared by diluting the stock solution with a suitable volume of deionized water to the desired concentration. The pH of the solution was maintained at a desired value by adding 0.1 M of NaOH or HCl.

3.2. Batch adsorption experiments

Batch adsorption experiments were carried out by batch process. Batch adsorption experiments examined the effect of solution pH, initial MB dye concentration, temperature, adsorbent dosage, and contact time on the MB dye adsorption. The experiments were carried out in a 250 ml Erlenmeyer flask and the total volume of the reaction mixture was kept at 100 ml.

3.2.1. Effect of initial dye concentration

0.1 g of adsorbent was placed in an Erlenmeyer flask with 100 ml volume of MB dyes solution. The initial concentrations of the dye solution were (5, 10, 15, 20, 25, 30, 40, 50) mg/L. the pH was adjusted at 7, The Contact time of experiment was fixed at 30 minutes, the stirring rate was 100 rpm and the temperature was 30^{o}C. The mixture was agitated and after the specified time the composite was attracted from the solution by a magnetic core then the concentrations of MB dye were analyzed using a spectrophotometer.

3.2.2. Effect of pH

The effect of initial pH was investigated at various pH (3, 4, 5, 6, 7, 8, 9, 10 and 12). 0.1 g of adsorbent was added to 100 ml volume of MB dye aqueous solution (initial concentration 10 mg/L), the temperature of Experiment was 30^{o}C and stirred at 100 rpm for a

constant sorption time of 30 minutes. The sample was taken and the composite was attracted from the solution by a magnetic core, and the equilibrium concentration of MB dye was then measured by spectrophotometer.

3.2.3. Effect of adsorbent dosage

A 100 ml volume of MB dye solution (10 mg/L) was mixed with various dosages of adsorbent (0.05, 0.1, 0.15, 0.2 g) at a contact time of 30 minutes, stirring rate was 100 rpm, Temperature was 30^{o}C and pH 7. After equilibrium the composite was attracted from the solution by a magnetic core, the concentration of MB dye was measured by spectrophotometer. The amount of MB dye adsorbed at equilibrium per unit mass of adsorbent q_e (mg/g) was determined according to the following equation:

$q_e = V (Co – Ce) / m$

Where Co is the initial concentration of MB dye (mg/L), Ce is the equilibrium concentration of MB dye (mg/L), V is the volume of

MB dye solution (L), m is the mass of adsorbent (g) and q_e is the

MB dye quantity adsorbed at equilibrium (mg/g). The percentage removal of MB dye dye was calculated as follows:

$\%R = (Co – Ce) / Co * 100$

3.2.4. Effect of contact time

0.1 g of adsorbent was added to 100 ml of 10 mg/L MB dye solution for various contact times (5, 10, 15, 20, 30, 40, 50, 60, 70, 80 and 90 minutes) at a constant pH 7, the stirring rate was 100 rpm and temperature of 30^{o}C. After the specified time the composite was attracted from the solution by a magnetic core then the residual MB dye concentration was measured by spectrophotometer.

3.2.5. Effect of temperature

0.1 g of adsorbent was added to a 100 ml volume of 10 mg/L MB and dye solution. The experiment were carried out at (25, 30, 35, 40, 50, 60 and 70^{o}C for 30 minutes contact time at stirring rate equaled 100 rpm and pH 7. After the specified time the composite was attracted from the solution by a magnetic core, the concentration of MB and dye was measured using a spectrophotometer.

3.2.6. Analytical technique

The equilibrium concentration of MB dye solutions before and after adsorption was analyzed using a UV-Vis spectrophotometer (Hach DR6000). The standard calibration curve of MB dye was prepared by recording the absorbance values of various concentrations of MB dye at the maximum absorbance wavelength (665 nm). The instruments used were a pH meter (HACH-HQ440d) and magnetic stirrer.

3.2.7. Adsorption isotherms models

Several isotherm models have been developed for evaluating the equilibrium adsorption of dyes from solutions such as Langmuir, Freundlich, and Temkin. The adsorption isotherms get their beneficial use from their applicability to describe the interaction between the adsorbate and the adsorbent of a given system. Several models can be used to analyze the experimental data to provide information about the adsorption mechanism as well as the adsorbent surface properties and affinities. The most accepted models for single solute systems are Langmuir and Freundlich models (Vargas *et al.* 2011; Langmuir, 1916; Freundlich, 1907).

2.3.2.7.1. The linear form of Langmuir equation can be expressed as follows:

$$\frac{Ce}{qe} = \frac{1}{Kl} + \frac{al}{Kl} + Ce$$

Where K_L and a_L are Langmuir constants that can be obtained from theintercept and slope of the straight line of the plot Ce/qe versus Ce. The $a_L$constant is related to the free energy or net enthalpy of adsorption (mg/L) ($a_L \propto e^{-\Delta H/RT}$)whereas K_L is the equilibrium constant of Langmuir (L/g).The constant q_{max} which equals K_L/a_L (mg/g) is the monolayer saturation capacity representing the maximum adsorption capacity of the adsorbent for a given adsorbate.

3.2.7.2. The linear form of Freundlich equation can be presented as follows:

$$\log qe = \log Kf + \frac{1}{nf} logCe$$

Where q_e is the equilibrium adsorption capacity which is the amount of adsorbed molecules per gram of adsorbent at equilibrium (mg/g), Ce is the solution equilibrium concentration (mg/L), K_f and n_f are the Freundlich parameters that represented the adsorbent affinity (mg/g) $(L/mg)^{1/n}$) and the heterogeneity factor, respectively. These parameters can be obtained from the intercept and slope of the straight line of the plot log q_e against log Ce.

3.2.7.3. The linear form of Temkin equation can be presented as follows:

$$q_e = \beta \ln\alpha + \beta \ln C_e$$

α is the equilibrium constant corresponding to the maximum binding energy : Lg^{-1}

$\beta = RT/b$

T is the absolute temperature in Kelvin

R is the universal gas constant 8.314 J $mol^{-1}K^{-1}$

b is the Temkin constant related to heat sorption /J mg^{-1}

α and β are calculated from the slope and intercept of q_e versus ln Ce

The experimental data of the adsorption isotherm for the two systems were analyzed by linear fitting to last models

3.2.8. Adsorption Kinetics

Kinetic of the adsorption process is vital to understand the dynamics of the adsorption reaction in terms of the order and the rate constant. Therefore, pseudo-first-order (Lagergren model), pseudo-second-order and intraparticle diffusion (Webber and Morris model) models were utilized in this study. Their linear equations are presented as follows:

Pseudo-first-order :

$\ln (q_e - q_t) = \ln q_e - k_1 t$

Pseudo-second-order

$$\frac{t}{qt} = \frac{1}{K2\ qe2} + \frac{t}{qe}$$

Intraparticle diffusion

$$qt = Ki\sqrt{t}$$

Where k_1 is the pseudo-first-order rate constant (min^{-1}), k_2 is the pseudo second-order rate constant (g/mg/min), k_i is the intraparticle diffusion model rate constant ($mg/g/min^{0.5}$), The experimental data of the adsorption kinetics for our systems were analyzed by linear fitting of these three models.

2.3.2.9. Thermodynamic Studies.

The spontaneity, feasibility and adsorbate-adsorbent interactions modes can be well understood via thermodynamic studies. Gibbs free energy (ΔG_o), Enthalpy change (ΔH_o) and Entropy change (ΔS_o) were calculated using mathematical relations:

$$lnK_o = \frac{\Delta S^\circ}{R} - \frac{\Delta H^\circ}{RT}$$

$$\Delta G^\circ = -RTlnK_o$$

$$\mathbf{\Delta G^0 = \Delta H^0 - T\,\Delta S^0}$$

Where T is the temperature in Kelvin, R is the gas constant and K_o can be obtained from equilibrium concentration and quantity adsorbed at equilibrium. The values of enthalpy (ΔH^o) and (ΔS^o) can be obtained from the plot of $\ln K_o$ versus 1/T.

3.2.10. Repeatability Study.

The repeatability of the (ASRHNMC) for adsorption of (MB) dye was investigated by analyzing five samples containing the same conditions of experiment, the same concentration of cationic dye (MB) 10 mg/l, the concentration of adsorbent dose (0.1g)/100 ml, and the same experiment conditions of (pH 7, Temp 30^{o}C, the same stirring rate 100 rpm and the same contact time 30 minutes). After the specified time the composite was attracted from the solution by a magnetic core then the residual MB dye concentration was measured by spectrophotometer.

3.2.11. Regeneration Study of composite after (MB) dye adsorption.

i-Adsorption Experiment of M.B.

Adsorption Experiment of (MB) dye was done by (ASRHNMC) adsorbent with applying the optimum conditions of adsorption process. The adsorbent dose was 0.1g/100 ml, the dye concentration was 10 mg/l, pH was 7, fixed stirring rate at 100 rpm, contact time was 30 minutes and the temperature was 30^{o}C. After adsorption of M.B, the nano-composite was attracted from the solution by a magnetic core then the residual MB dye concentration was measured by spectrophotometer.

ii-Desorption Experiment of M.B.

(ASRHNMC)-M.B was attracted from the solution by a magnetic core after adsorption, immersed in 100 ml of(0.1M) NaOH with shaking by vortex instrument for 5 minutes and repeated several times. Then the adsorbents were washed several times with deionized water and dried in oven at 105^{o}C till dryness.

The experiment of adsorption /desorption was repeated with the same conditions for four cycles.

RESULTS AND DISCUSSION

1. Characterization

1.1. Point of zero charge (pH_{pzc})

The point of zero charge (pH_{pzc}) of (ASRH) was 7 (Fig. 1a) and that of (N.M) was 4 (Fig. 1b). This result is in agreement with (Zhang *et al.*, 2020) who found that the isoelectric point (pH_{pzc}) value was between (3.0 – 4.0). In an aqueous system, the surface of iron oxides is covered with groups of –FeOH, etc. When the pH value was below or above the (pH_{pzc}), hydroxyl groups of –FeOH on the surface would be changed to functional groups of $FeOH_2^+$ or FeO^- by protonate and deprotonate. The balance of protonation and deprotonation depended on the pH of the solution and (pH_{pzc}) of Fe_3O_4 (Zhang *et al*., 2020).

In the present study, pH= 5.7 has been chosen because it is in the middle of the two values, so when (ASRH) sample immersed in an aqueous solution had the pH= 5.7 which is lower than it's (pH_{pzc} = 7), the (ASRH) gained surface (-ve) charge. In contrast when (N.M) sample which has (pH_{pzc} = 4) immersed in an aqueous solution had the pH= 5.7 which is higher than its (pH_{pzc}), its surface gains (+ve) charge. So attraction force takes place between (-ve) charged surface molecules of (ASRH) composite and (+ve) charged surface molecules of (N.M) to form the Nano-Magnetite Composite (ASRHNMC).

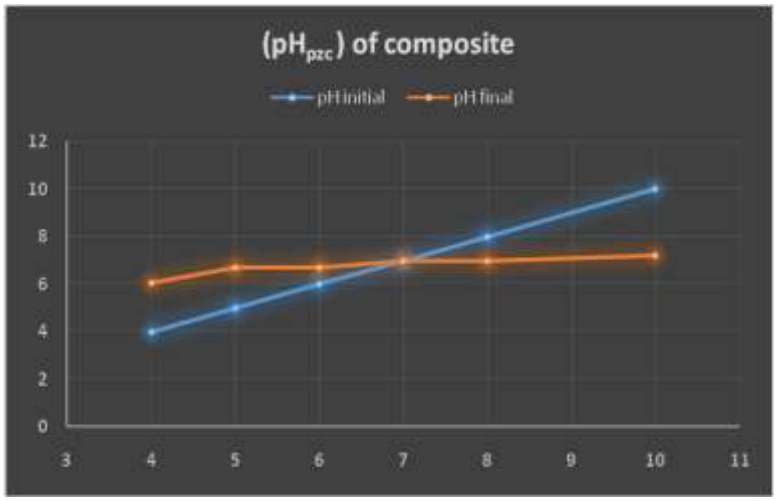

Fig. (1a). Point of zero charge (pH_{pzc}) of (ASRH)

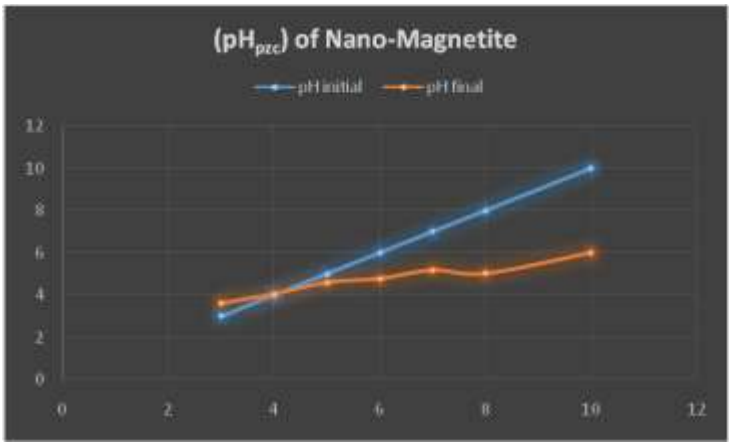

Figure (1b)Point of zero charge (pH_{pzc}) of (N.M).

1.2. X-ray diffraction pattern (XRD)

The crystallinity of (N.M), (AS) and (ASRHNMC) was studied through the XRD analysis for determining the structural changes in the developed adsorbent samples before and after improvement.

The magnetite sample was characterized by X-ray powder diffraction (XRD) with the corresponding results displayed in Fig. (2a). the diffraction pattern and the relative intensities of all the diffraction peaks are typical of the magnetite and match those synthesized in this research. The diffraction peaks with (2θ) at 30.0, 35.6, 48.3, 57.2 and 62.5 are observed, which indicate that the Fe_3O_4 particles have an amorphous structure and that was in agreement with (Fatemeh *et al.*, 2013). Furthermore, the sample shows some of the

characteristics of the bulk magnetite crystallite phase, with the broad peaks suggesting the nano-crystallite nature of the magnetite particles (Liliana *et al.*, 2013). The resulting mean particle diameter of magnetite nanoparticles, as calculated from the Scherrer equation, was ca. 11.6nm.

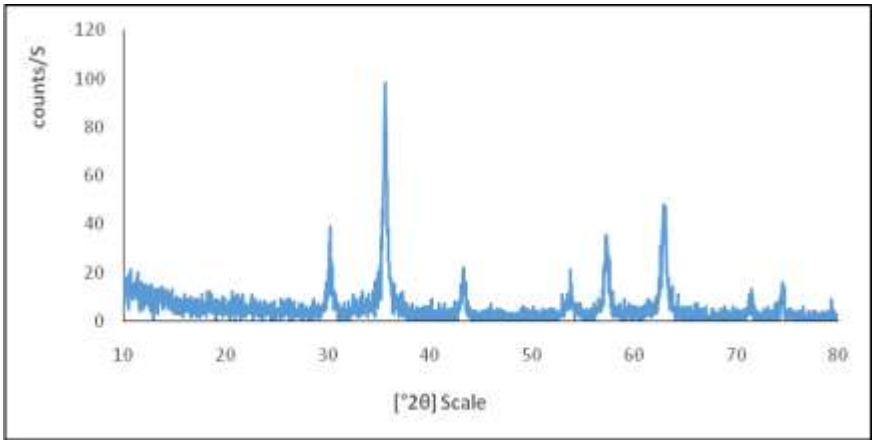

Fig. (2a). XRD spectrum of Nano-Magnetite (N.M).

The XRD pattern of the water treatment plant sludge (AS) shown in Figure (2b) indicates the presence of two major amorphous phases, namely, silica [SiO_2] and albite [Na Al Si_3 O_8]. These results indicate that the water treatment plant sludge presents, in its composition, minerals that are similar to those commonly occurring in clays. (Raseid*et al.*, 2016; Hegazy *et al.*, 2012)

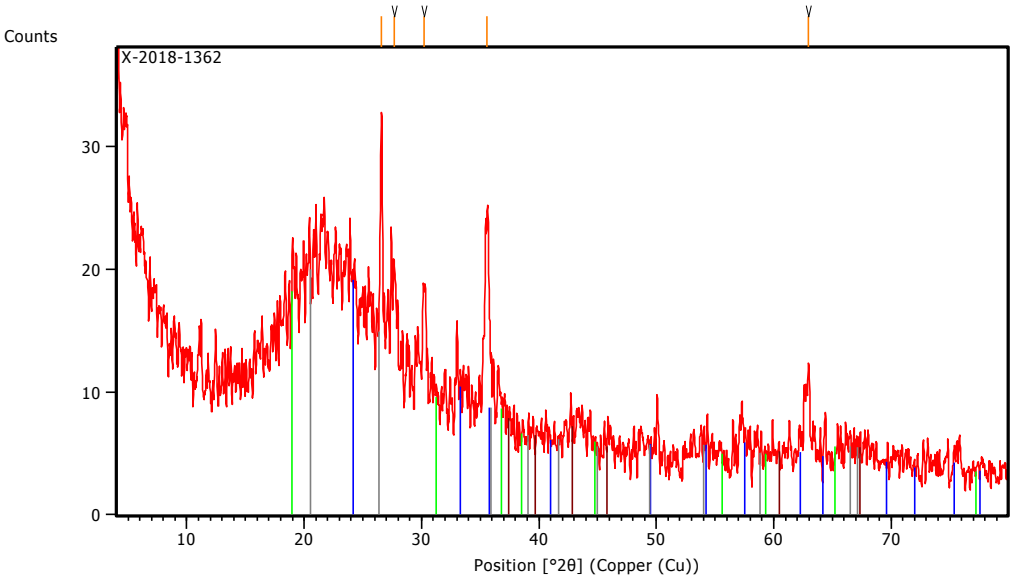

Figure (2b). XRD spectrum of (AS)
01-085-1780 - [SiO2] - Silicon Oxide.
00-001-1243 - [Na Al Si_3 O_8] - Albite

Figure (2c) shows the XRD patterns of the composite. The same signals of silica [SiO_2] and albite [Na Al Si_3 O_8] in the same values of [°2θ] were appeared in both samples of (AS) and (ASRHNMC) which indicates the stability of these compounds with activation by

heat at 700^{o}C and addition of rice husk which increase the amount of amorphous silica these results are in agreement with (Raseid*et al.*, 2016; Hegazy *et al.*, 2012). The intense broad peak observed at around [°2θ] = 20 and the peak at [°2θ] = 26.7 for both (AS) and (ASRHNMC) sample indicatesthat a high percentage of these particles are amorphous, but a few of them are crystalline. (Deshmukh, P., *et al.*, 2012) and that result confirms that the temperature of calcination (at 700^{o}C) was optimum to form amorphous silica from rice husk added to sludge for improvement and also that temperature did not effect on the amorphous phase of silica of alum sludge during calcination.

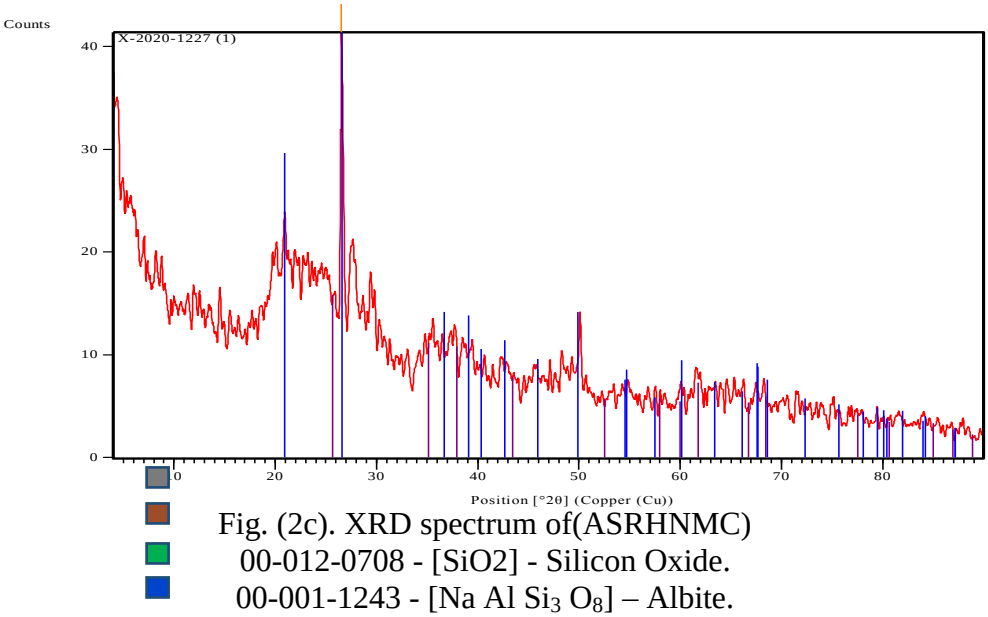

Fig. (2c). XRD spectrum of(ASRHNMC)
00-012-0708 - [SiO2] - Silicon Oxide.
00-001-1243 - [Na Al Si_3 O_8] – Albite.
00-026-1136 - Fe_3O_4 - Iron Oxide - Magnetite.
00-001-1053–Fe_2O_3 - Iron Oxide - Hematite.

In the nano-composite sample, besides the broad band characteristic for the presence of the amorphous silica and albite, the amorphous nano-magnetite characteristic bands were evidenced. This could be assigned to the bonding of the iron into Si-O-Fe-O-Si polymeric bonds that do not break at low temperatures. The results are in good agreement with the result reported by (Rafique *et al.* 2014).

3.1.3. Fourier transform infrared spectrophotometer (FT-IR)

It was clear from Figure (3a) that the bands at 445 cm^{-1}and 467 cm^{-1}were assigned to Si-O-Si bond vibration Symmetric stretching vibrations of Si-O-Si belonging to ring structures. The absorption bands at 1089.68 cm^{-1} is due to Asymmetric stretching vibration of Si-O-Si. The absorption bands at 1646 cm^{-1} is due to Combination of vibrations of the SiO_2network. The bands at 3440 cm^{-1} is due to Si-O-H and O-H bonds in surface water molecules that results are in good agreement with the results reported by (Rafique *et al.*, 2014). The absorption band present at 2928-2962.18 cm^{-1} may suggest the presence of organic carbon these bands are due to C-H absorption contaminants present in the sample. It can be inferred that the alkane groups play a significant role in adsorption as their adsorption peak 2927.96 cm^{-1} characteristic of carbon-and hydrogen containing species, with double bond and are assigned to various forms of C-H stretching, and CH_2alkene. Calcite is the most common carbonate mineral in natural samples the existence of peak at 1412cm^{-1}. The peak at 785 cm^{-1}are observed for albite. The observation of the peak in the range 531.52 cm^{-1}

indicates the presence of albite ($NaAlSi_3O_8$; Na- feldspar).These results are in agreement with (Raseid*et al.,* 2016).

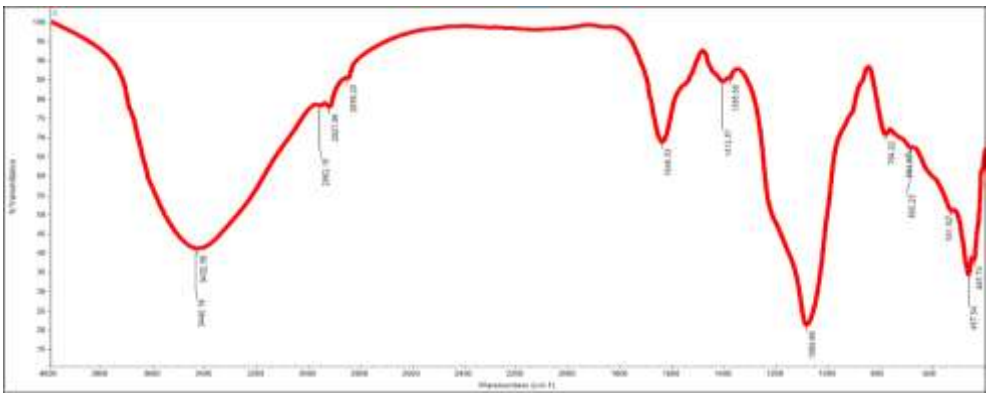

Fig. (3a). FT-IR spectrum of Alum Sludge (AS)

Study of data in Figure (3b) reveals that the sample exhibits two intense peaks, respectively at 582 and 637.20 cm^{-1} bands, that are due to the stretching vibration mode associated to the metal–oxygen absorption band (Fe–O bonds in the crystalline lattice of Fe_3O_4) (Ahn. *et al.,* 2003). They are characteristically pronounced for all spinel structures and for ferrites in particular. This occurs because of the contributions, in these regions, deriving from the stretching vibration bands related to the metal in the octahedral and tetrahedral sites of the oxide structure. The absorption bands at 3422, 3157.45 and 1622 are due to stretching and bending vibrations of (O-H bonds) in surface water molecules (Rafique *et al.,* 2014). Thus the absorption bands shown by the synthesized iron oxide are in good agreement with the reported absorption bands of magnetite type of iron oxide.

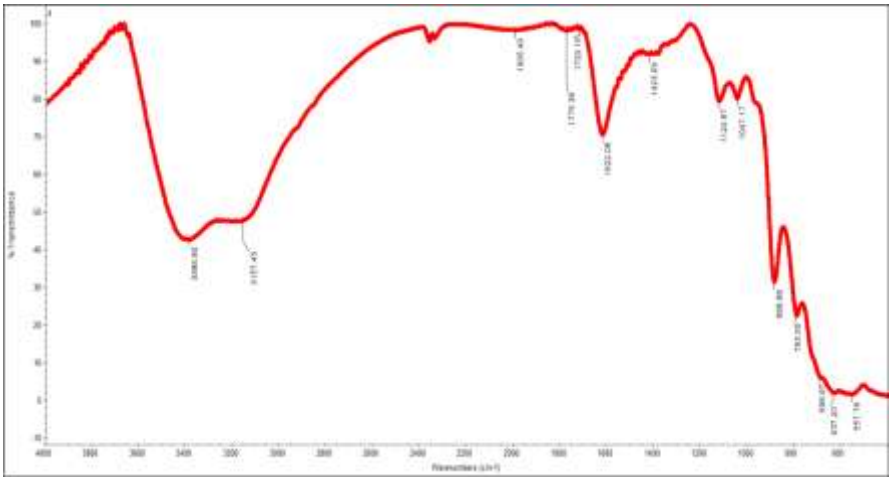

Fig. (3b). FT-IR spectrum of Nano-Magnetite (N.M).

Figure (3c) shows that the bands at around 1639.92 cm^{-1} and 3444.67 cm^{-1}can be assigned to the H-O-H stretching modes and bending vibration of the free or adsorbed water, respectively. The band at 469.22 cm^{-1} and 582$cm^{-1}$is related to the Fe-O bending vibration and are attributed to the formation of the ferrite phase. That is in good agreement with the results reported by (Fatemeh *et al.,* 2013) and that was the same bands appeared at FTIR spectrum of Nano-magnetite.

The broad high-intensity band at 1094cm^{-1}is associated with the motion of oxygen in Si-O-Si ant symmetric stretch, due to the asymmetric stretching bonds of Si-O-Si in SiO2.801.07 cm^{-1} band were assigned to Si-O-Si bond vibration Symmetric stretching vibrations of Si-O-Si belonging to ring structures.

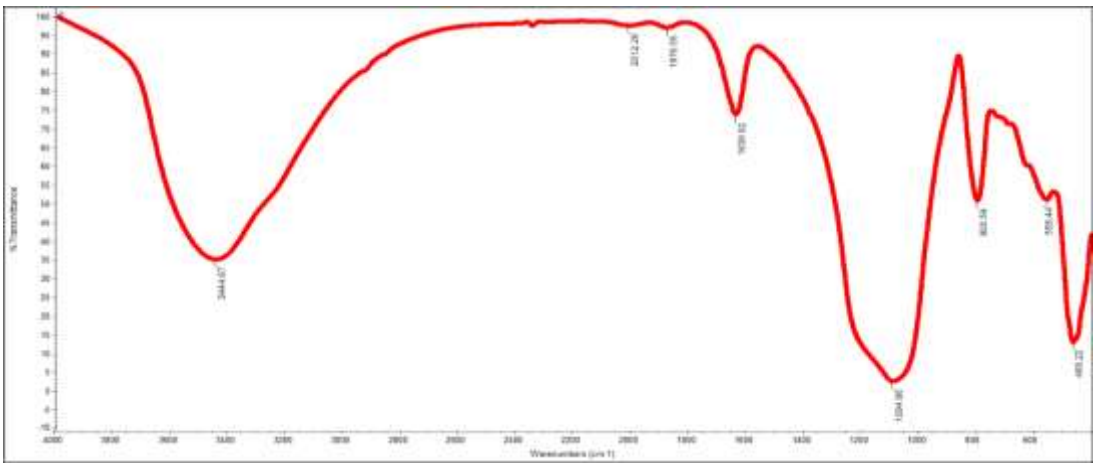

Fig. (3c). FT-IR spectrum of (ASRHNMC).

3.1.4. Energy dispersive X-Ray spectroscopy (EDX)

The elemental composition of the (AS) and the synthesized Nano-Magnetite composite (ASRHNMC) were investigated by EDX technique. EDX pattern of (AS) (Fig 4a) shows that, the weights of silica 31.63% and 1.22%, Alumina 8.92 %, iron 1.92 % and two beaks of Calcium at 15.07% and 2.1%. In EDX pattern of (ASRHNMC) sample (figure 4b)shows that, the weights of silica was become 45.2% and 1.72%, the clear appearance of iron band, due to the improvement with Nano-Magnetite impregnated into the composite with iron weight 8.38% and 2.5%, Alumina weight was 6.16%, weight of Sulfur was 1.72% and chloride 0.79%.

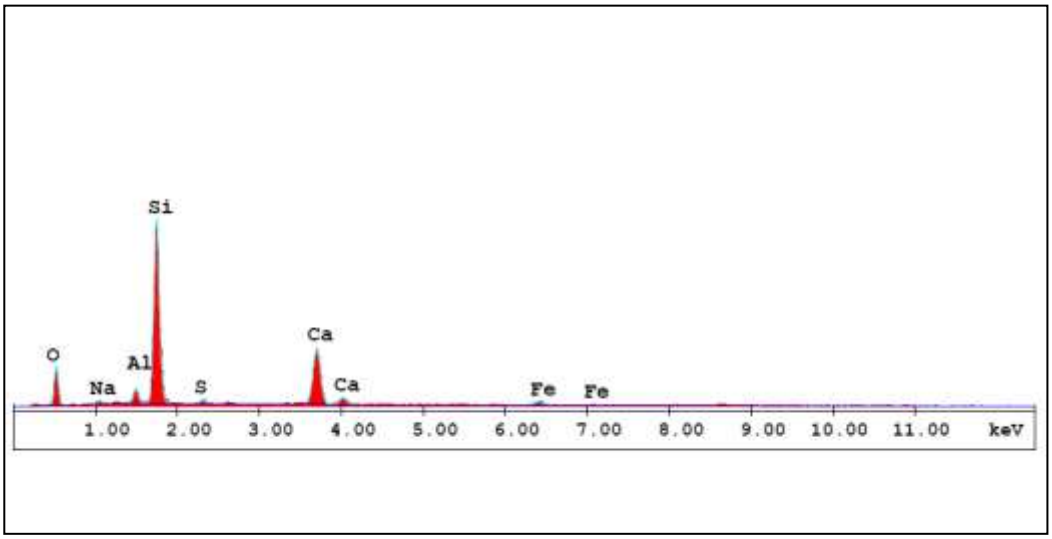

Fig. (4b): The EDX of (AS)

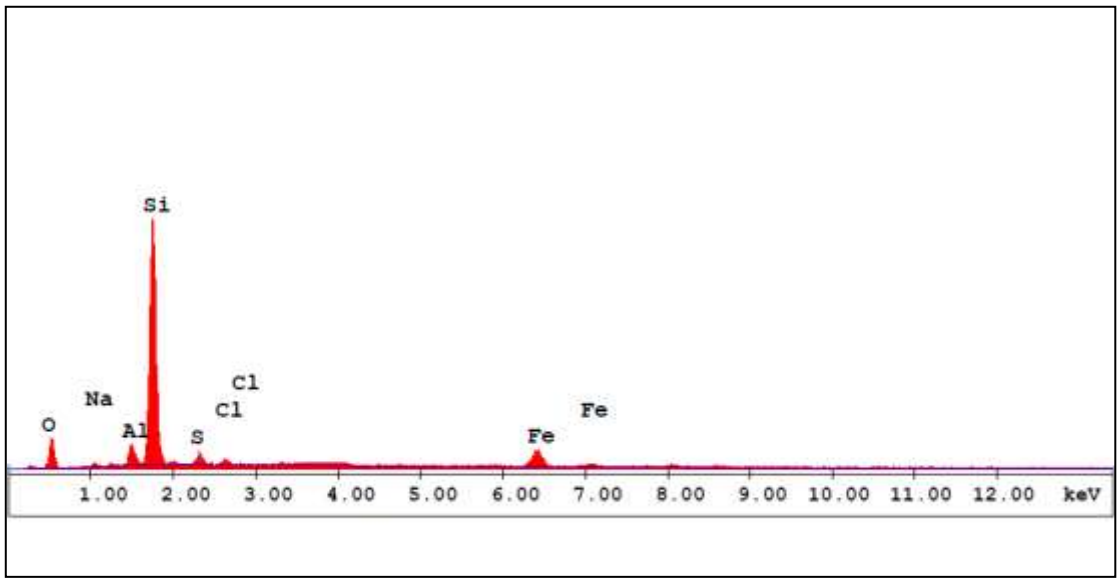

Fig. (4b): The EDX of (ASRHNMC)

3.1.5. Scanning electron microscope (SEM)

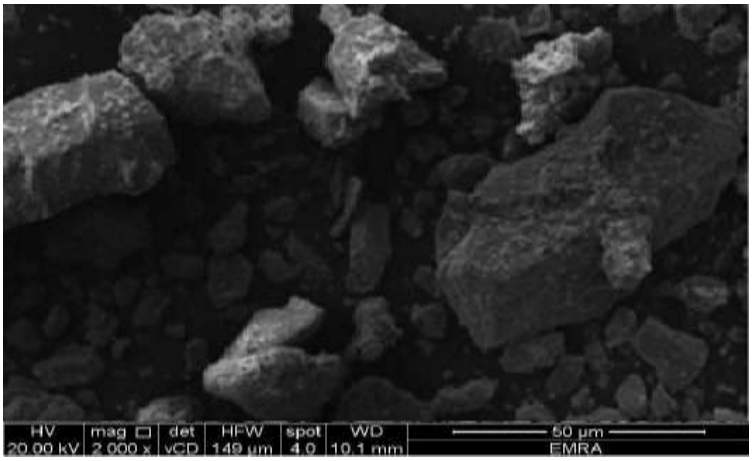

Fig. (5a).| SEM images of alum sludge (AS) magnified by 2000x.

The morphology of composite (ASRHNMC) was studied by SEM, Fig.(5b)Very fine micro particles were observed with diameter 0.2-0.8 µm in the SEM of nano-composite (ASRHNMC). Presence of these fine particles leads to increase in the porosity and the surface area of the modified Alum Sludge. This was confirmed by the measured surface area obtained for composite (ASRHNMC) = (126.4 m^2g^{-1}) compared to (AS) = (62.56 m^2 g^{-1}). Also the image clearly shows the formation of porous material in (ASRHNM) as a composite material with nano-magnetite and mesoporous SiO2.Images indicated that surface of improved alum sludge was modified with magnetite nanoparticles in nanometer range and gave it magnetic properties.

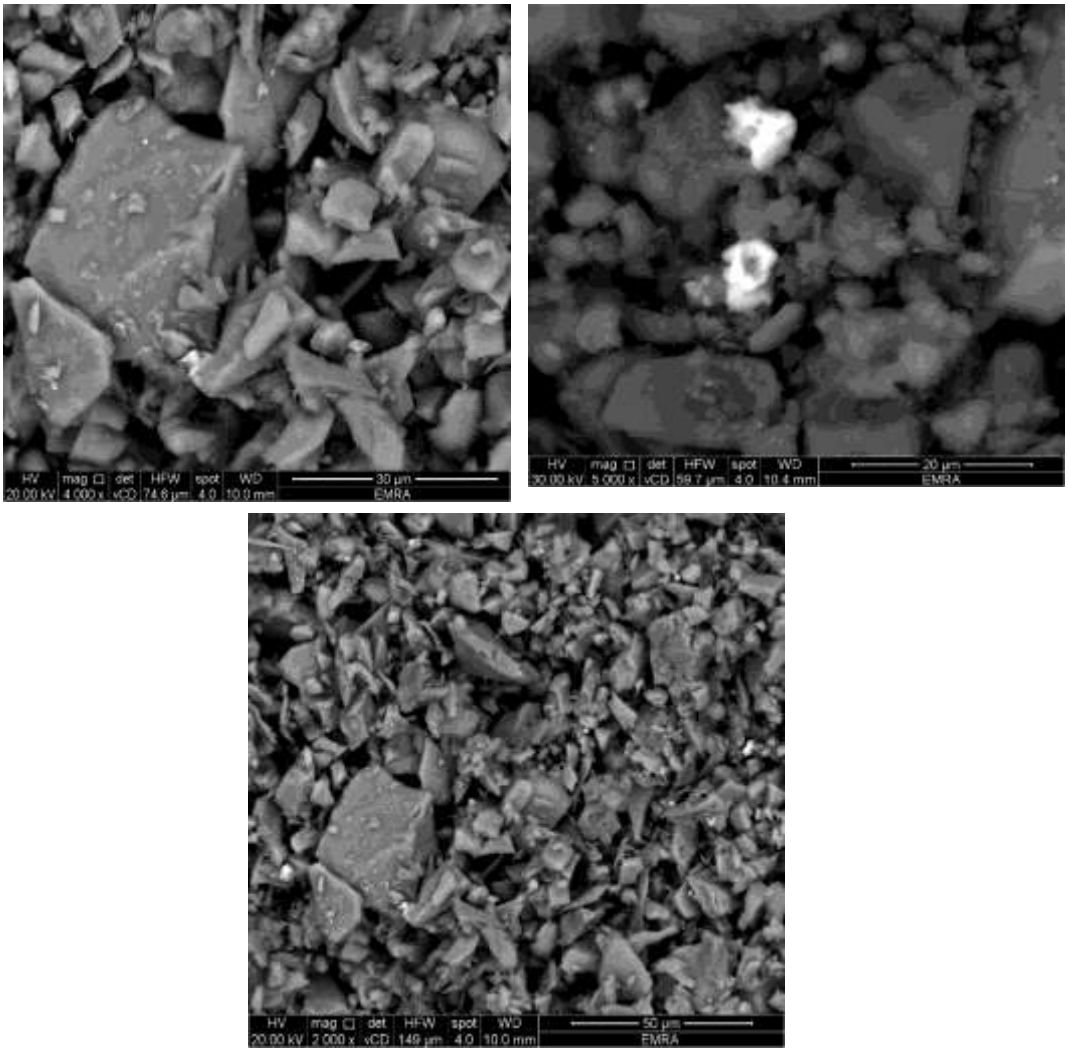

Fig. (5.b) | SEM images of (ASRHNMC) magnified by 2000x, 4000x and 5000x.

3.1.6. Transmission electron microscopy (TEM)

From Figure (6a) and from the corresponding electron diffraction pattern, it was determined that the magnetite particles are spherical with an average diameter of 9 nm.

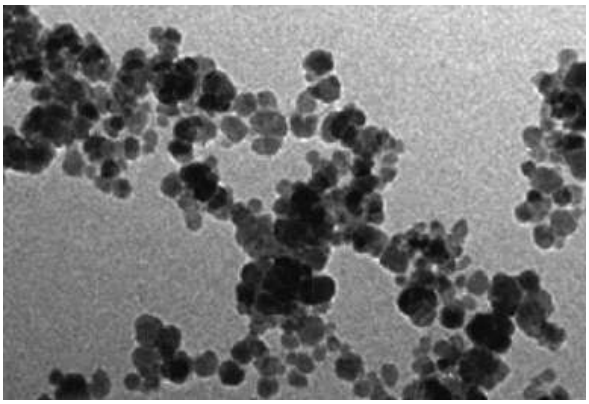

Fig. (6a). Transmission electron microscope (TEM) image for magnetic Fe_3O_4 nanoparticles synthesized.

It was clear from Figure (6b) that the nano-magnetite was impregnated into the mesopore structures. Coagulated nano-magnetite formed backbones with well-organized and aligned mesopores. Particle sphere like structure.

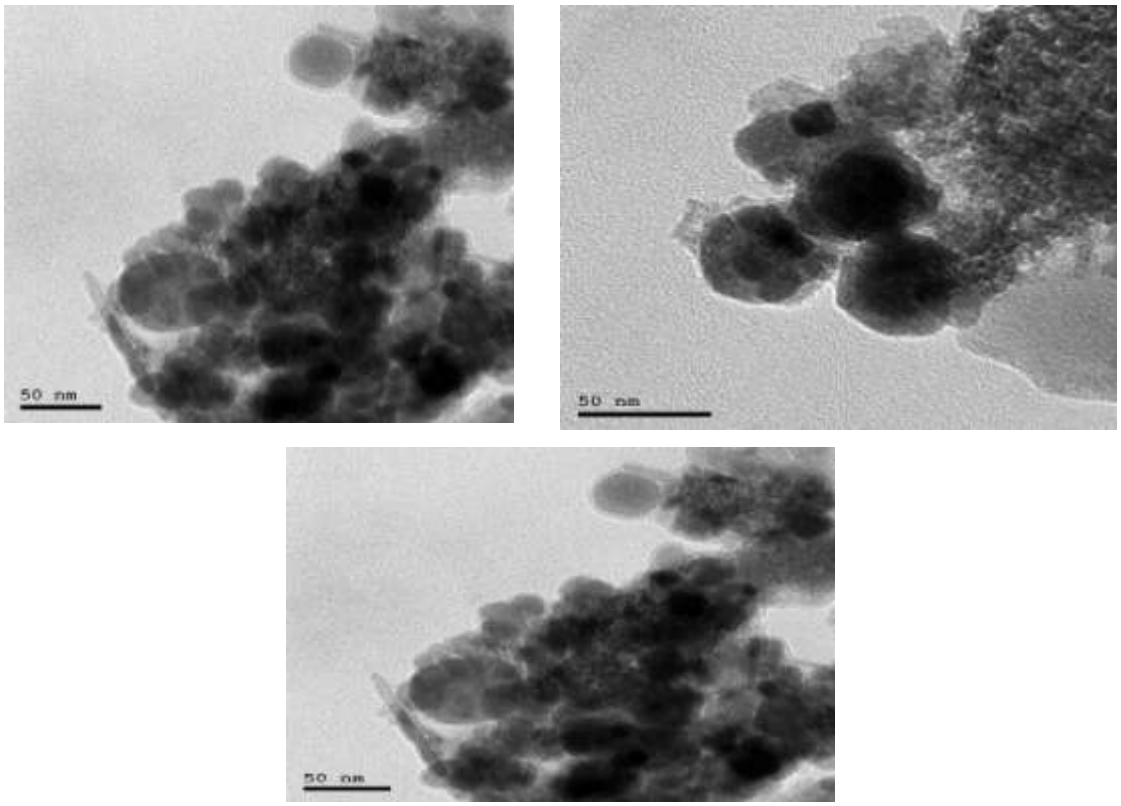

Fig. (6b) Transmission electron microscope (TEM) image for (ASRHNMC).

3.1.7. The Brunauer-Emmett-Teller (BET) specific surface area

The N adsorption–desorption isotherm of (ASRHNMC) obtained under optimum conditions are shown in Figure (7). The adsorption-desorption isotherm is classified as type II with H3 hysteresis loop referred to slit-shape pore structure

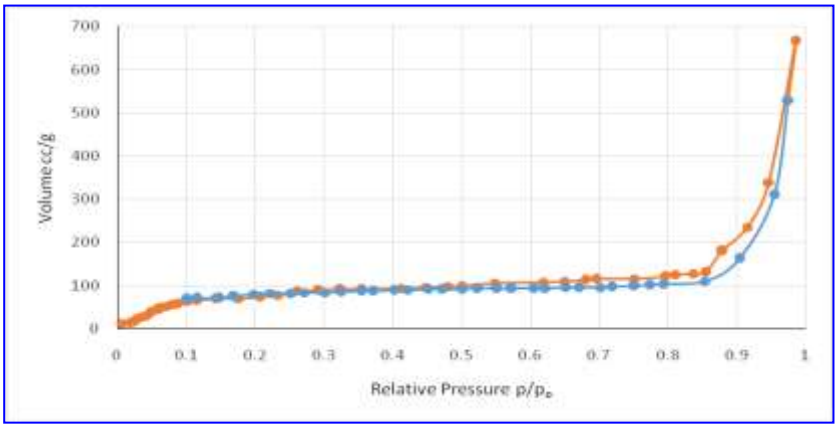

Fig. (7). N adsorption–desorption isotherm of (ASRHNMC)

The BET surface area and pore volume were calculated according to the BET specific surface Formula for (AS), (ASRH) and (ASRHNMC) as shown in Table (1). We found that the BET surface area of (AS) was 62.56 m^2/g and that is agree with (Lee *et al.,* 2006) who found that the specific surface area of dried alum sludge was 61 m2/g. The result is disagree with (H. F. Wu, *et al.*, 2019) who found that the specific surface area of alum sludge was 31.564 m^2/g. This confirms that the specific surface areas of alum sludge in various water plants differ (Wang *et al*., 2016). And alum sludge characteristics are influenced by the quality of the drinking water source, coagulant type, and treatment plant system (Siswoyo *et al*., 2014).

Table (1). BET surface data of (AS), (ASRH) and (ASRHNMC).

sample	S_{BET} (m^2/g)	Pore volume (V_p) (cm3/g)	Average pore size(r_p) (nm)
A.S	62.56	0.05582	1.82
ASRH	138.22	0.1925	2.41240
(ASRHNMC)	126.402	0.16091	2.15288

The BET surface area of (ASRH) was 138.22 m^2/g and the Pore volume was 0.1925cm3/g which are more greater than that of (AS) due to the thermal treatment of alum sludge at 700^{o}C with rice husk which increase the amorphous silica content characterized with large surface area and mesoporous structure, also the thermal treatment make some fusion to the sludge content and destroys organic contaminants. Moreover The increased surface area of rice husk modified (ASRH) sample is mainly attributed to the combustion of rice husk organic components leaving several pores, the dimensions (average pore radii, r_p nm and pore volume, V_p cm^3/g) of which are controlled by concentration and homogeneity of rice husk fiber distribution (Nasser H. Shalaby *et al.*, 2017). So the average pore size in (ASRH = 2.412 nm) increased markedly than (AS = 1.82 n.m).

The BET surface area of (ASRHNMC) was 126.402 m^2/g which is larger than (AS = 62.56 m^2/g) but smaller than (ASRH = 138.22 m^2/g) and the Pore volume was 0.16091cm^3/g which is greater than that of (AS) but smaller than (ASRH). The average pore size decreased in (ASRHNMC) to 2.15288n.m which is smaller than (ASRH= 2.41240 nm) but larger than (AS =1.82 nm). The average pore size of both (ASRHNMC) and (ASRH) reveals that both composites are of mesoporous while in case of (AS) is considered of microborous and that explains the larger adsorption capacity of both composites than (AS). The presence of nano-magnetite as a constituent in the (ASRHNMC) composite caused a decrease in the specific surface area, the pore size and pore volume of composite by the introduction of the nano-magnetite in the pore frameworks (Kittappa, S. *et al.*, 2015).

3.1.8. X-ray fluorescence (XRF) spectrometer

Table (2). XRF Results for (AS at 105^{o}C and 700^{o}C) samples, (RH) at 700^{o}C and (ASRH).

Element Oxide	**(AS) dried 105^{o}C**	**(AS) at 700^{o}C**	**(RH) at 700^{o}C**	**(ASRH)**
SiO_2	**38**	**49.93**	**99.20**	**73.55**
$AL2O_3$	**23.5**	**31.603**	**0.51**	**15.8**
Fe_2O_3	**3.63**	**5.26**	**0.04**	**2.43**
CaO	**4.42**	**6.326**	**0.05**	**2.96**
MgO	**1.37**	**2.015**	**0.03**	**0.92**
SO_3	**0.52**	**0.734**	**0.02**	**1.06**
Cl	**0.88**	**1.05**	**0.01**	**0.59**
Na_2O	**0.50**	**0.726**	**ND**	**0.37**
K_2O	**0.50**	**0.607**	**0.04**	**0.34**
TiO_2	**1.201**	**1.749**	**ND**	**0.977**
L.O.I	**26.68**	**-----**	**0.12**	**1.02**

3.1.9. Magnetic properties of Nano-Magnetite

Figure (8).Shows the magnetization curve of Nano-Magnetite (N.M) from the VSM obtained at 300 K corresponding to the MNP, presenting a magneticsharp TC in a nanoparticle (Victor *et al*., 2020). When one or more dimensions in the system are extremely small (below 50 nm), the growth of the spin correlation length will be eventually limited by the smallest dimension and the system will display a reduced transition temperature (TC) following the known finite-size scaling effect (Victor *et al*., 2020).

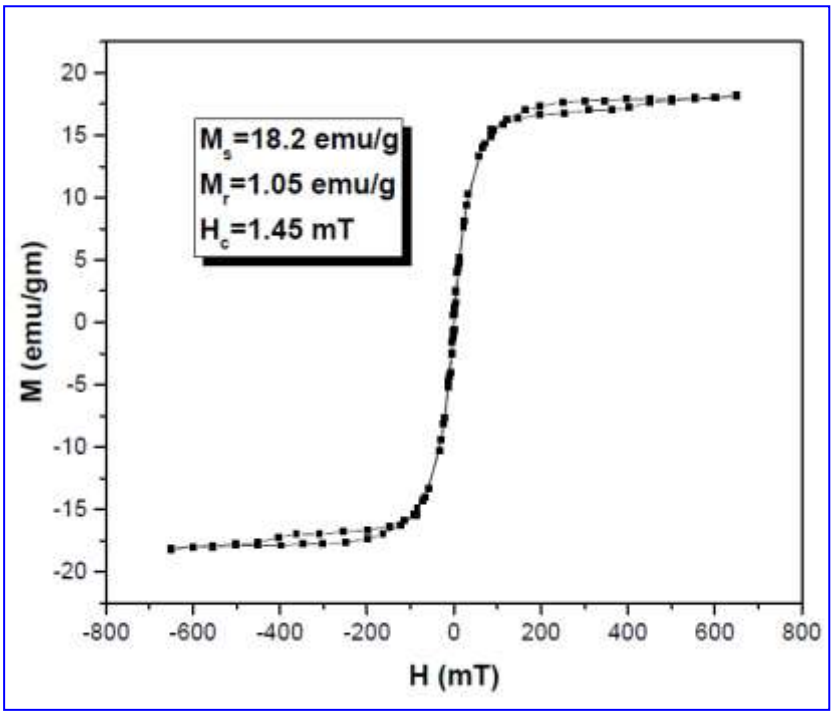

Fig. (8) Shows the magnetization curve of Nano-Magnetite (N.M)
Magnetization = 18, Crystal size = 11.6 n.m

3.2. Adsorption Studies.

3.2.1. Effect of initial dye concentration on adsorption

It was observed from the results that pH significantly influence the adsorption process. The adsorption data for removal of MB by the composite at various pH (3, 5, 6, 7, 8, 9, 10, 11 and 12) under fixed experimental conditions (adsorbent dose, 0.1 g/100 ml, contact time 30min., solution temperature 30^{o}C, and initial concentration 10 mg/L) are represented in Figure (9).

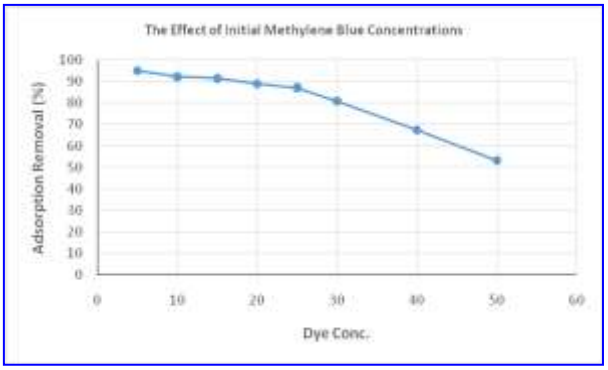

Fig. (9). Effect of Initial Methylene Blue Concentrations

The adsorption data for the removal of MB by the composite at different MB concentrations (5, 10, 15, 20, 25, 30, 40 and 50 mg/L) with fixed experimental conditions (adsorbent dose 0.1 g/100 ml; contact time 30 min; solution temperature 30^{o}C; pH 7 stirring speed 100 rpm) are represented in Figure (9). Thus, by increasing the initial concentration of methylene blue, the removal efficiency could be decreased. The removal efficiency 94.96% was obtained at an initial concentration 5 mgL^{-1}. After increasing the methylene blue concentration to 50 mgL^{-1}, the removal efficiency decreased to 53.48%. This result is consistent with the results obtained by Khalilollah and Seyed (2019) who reported in their study on the removal of methylene blue by rice husk silica adsorbent that the efficiency will be reduced if the initial concentration of methylene blue is increased. They proved that for a contact time of 60 minutes, an adsorbent dose of 1 gL^{-1}, pH 8, and an increase in the concentration from 10 to 100 mgL^{-1} reduced the removal efficiency from 96.7% % to 60.8%. This may be due to a decrease in the active level of adsorbent surfaces. In high concentrations, active bands are less available to pollutants and therefore the speed of mass transfer in these concentrations is reduced. In other words, at low concentrations the ratio of available surface to the initial concentration of pollutants is larger and thus the removal becomes independent of initial concentrations. However, in the case of higher concentrations, this ratio is low and therefore the removal efficiency depends on the initial concentration (Dejene *et al.*, 2016).

3.2.2. Effect of pH on Adsorption

It was observed from the results that pH significantly influence the adsorption process. The adsorption data for removal of MB by the composite at various pH (3, 5, 6, 7, 8, 9, 10, 11 and 12) under fixed experimental conditions (adsorbent dose, 0.1 g/100 ml, contact time 30min., solution temperature 30^{o}C, and initial concentration 10 mg/L) are represented in Figure (10). The results showed that the removal percent of MB by the composite increased with an increase in pH from 3 to 7.The removal of MB by the composite increased from 53.52 % to 90.67 % with increasing pH. Then the removal percent of MB by composite decreased with the increase in pH from 7 to 12. The removal of MB by the composite decreased from 90.67% to 61.68% with increasing pH from pH 7. So, the maximum uptake of MB dye was observed at pH 7. This phenomenon was similar to previous results reported by Kuai *et al* (2014) and (Zhao *et al.*, 2008).

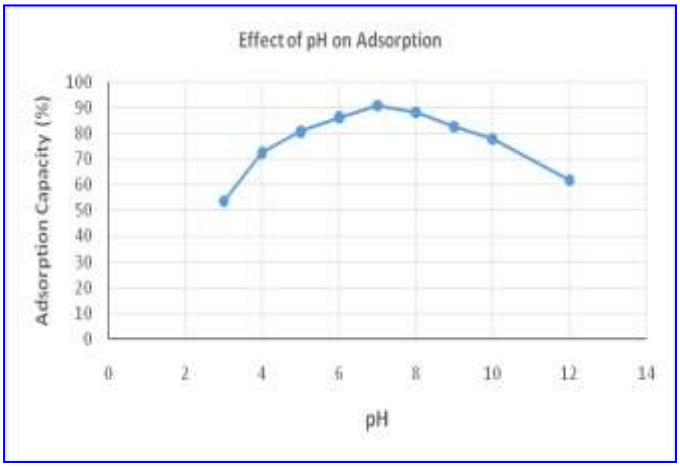

Fig. (10). Effect of pH on Adsorption of Methylene Blue

MB is a cationic dye, which exists in aqueous solution in the form of positively charged ions. The low adsorption of MB at an acidic pH was suggested to be due to the

presence of excess H^+ ions that compete with the dye cation for adsorption sites. The number of positively charged sites decreases, while the number of negatively charged sites increases, which favours the adsorption of MB due to electrostatic attraction. As the pH value increased from 7–12, the efficiency of the dye removal decreased. At higher solution pH, the decrease in the adsorption rate is due to the formation of a hydroxyl complex between the adsorbent and the dye (Raseid*et al.*, 2016).

3.2.3. Effect of initial composite dose on dye Adsorption

The experimental data for removal of MB by composite at different dosages (0.05, 0.1, 0.15 and 0.2 g/100 ml) with fixed conditions of (initial dye concentration 10 mg/L, contact time 30 min., solution temperature 30^{o}C and pH 7) are represented in Figure(11). It was clear that by increasing the adsorbent dose from 0.05 to 0.2g/100 ml the removal percent of MB by adsorbent increased from 85.05% to 92.72% so the effective adsorbent dose for the highest MB removal was (0.1g/100 ml). that was agreed with Raseid*et al.* (2016) found that the removal percentage of MB by the physically treated alum sludge by pyrolysis at 700^{o}C increased from 24.8 to 75.68% with an increase in the adsorbent dose of adsorbent from 0.05 to 0.25 g/100 ml); this can be attributed to the increase in adsorbent surface area and the availability of more adsorption sites resulting from the increase dosage of adsorbent.

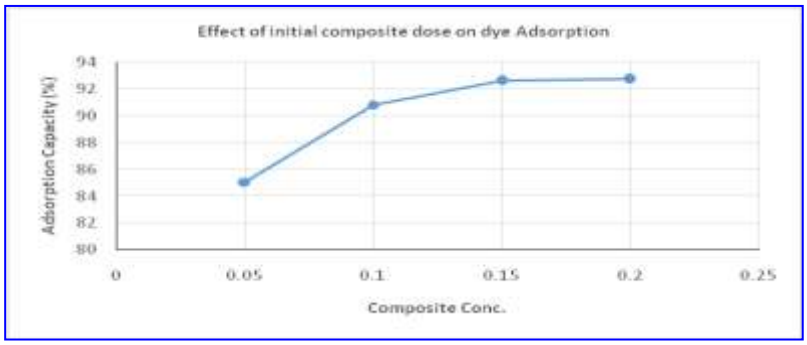

Fig. (11).The effect of adsorbent mass on MB removal efficiency by composite.

3.2.4. Effect of Contact Time on dye Adsorption:

The adsorption data for removal of MB dye by adsorbent at different contact times (5, 10, 15, 20, 25, 30, 40, 50, 60, 70, 80 and 90 min.) with fixed experimental conditions (initial dye concentration 10 mg/l, adsorbent dosage 0.1 g/100 ml, solution temperature 30^{o}C, and pH 7 and 100 rpm of stirring) are represented in Figure (12).The results showed that the removal efficiency of MB on the adsorbent increased with increasing time from 5 to 30 min and remains constant up to 90 min. So 30 minutes contact time was enough to achieve maximum adsorption of MB on the surface of composite. It can be concluded that MB was adsorbed onto composite very rapidly within 5–30 minutes; the fast adsorption in the initial stage may be due to the higher driving force creating a fast transfer of MB dye to the surface of the adsorbent particles and the availability of the uncovered surface area and active sites on the adsorbent; with increasing time the availability of uncovered surface area and the remaining active sites decreased. Ramavandi and Leili (2015) made a study on the adsorption of MB from aqueous solutions by shrimp shells. They found that any increase in the contact time would increase removal efficiency. Also, Khalilollah and Seyed (2019) reported that the amount of MB removal onto Rice Husk Silica Adsorbent increased for a contact time of 30 min from 72.4% to 93.4% for a contact time of 90 minutes.

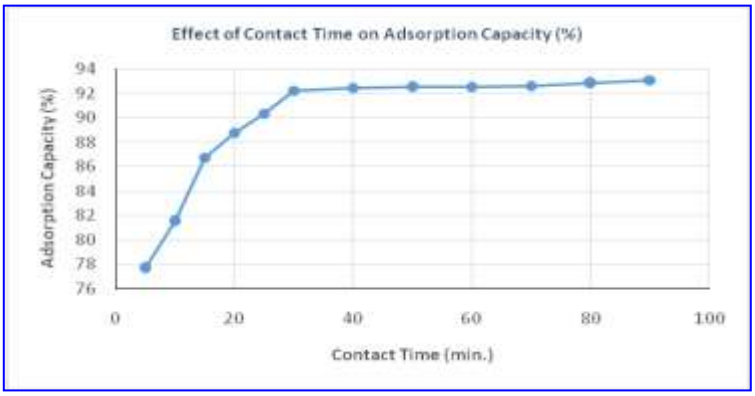

Fig. (12). Effect of contact time on MB dye removal by composite.

3.2.5. Effect of Temperature on Adsorption rate of MB dye:

The adsorption data for removal of MB dye by composite at different solution temperatures (25, 30, 35, 40, 50, 60 and 70^{o}C) at fixed experimental conditions (initial MB concentration 10 mg/L, adsorption dosage 0.1 g/100 ml, contact time 30 min, pH 7 and 100 rpm stirring) indicated that the increase in solution temperature from 25^{o}C to 60^{o}C highly increase the removal percent of MB by composite. The increase in adsorption with the rise in temperature may be due to the increase in molecular diffusion or may be attributed to the availability of more active sites on surface area. Higher percentage of removal at 60^{o}C compared to 25^{o}C might be due to the increase in mobility of the molecule dye (Ghasemi *et al.*, 2016). The adsorption of MB dye was an endothermic process as reported Ghasemi *et al.* (2016). However, Agarwal *et al.* (2016) documented that the rate of diffusion of the dye molecules across the external boundary layer and the internal pores of the sorbents particle increases when temperature increased due to the decrease in the viscosity of the solution. This might explain lower removal of MB in the present study when temperature increased from 60^{o}C to 70^{o}C as more MB molecules diffuse from the sorbent.

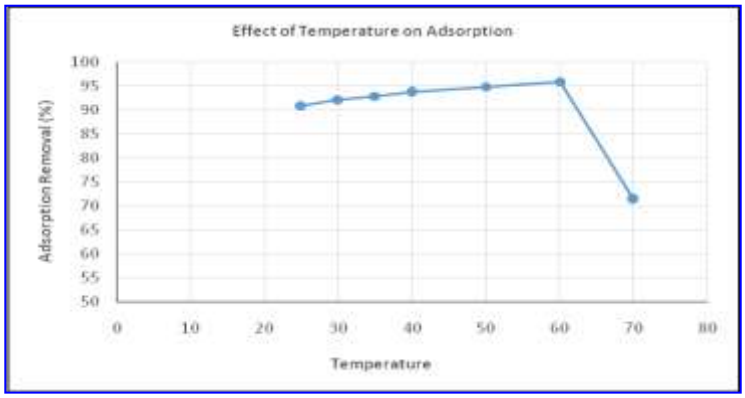

Fig. (13). Effect of temperature on MB removal using Composite.

3.2.6. Thermodynamics Study for MB dye:

The temperature has two major effects on the adsorption process. Higher temperature increases the rate of diffusion of the adsorbate molecules across the external boundary layer and in the internal pores of the adsorbent particle, owing to decrease in the viscosity of the solution. In addition, temperature changing will change the equilibrium capacity of the adsorbent for the particular adsorbate. In this case of study, a series of experiments was conducted at 303, 313, and 323 K to study the effect of temperature on the adsorption rate.

The results indicated that adsorption increases with the temperature (Fig. 14) which indicates the endothermic nature of the adsorption process. Similar result was reported for MB adsorption onto magnetized nanocomposite mesoporous silica (Kittappa *et al.*, 2015).The standard deviations (σ) at 303, 313, and 323 K were found to be 14.43, 10.97 and 9.33 respectively.

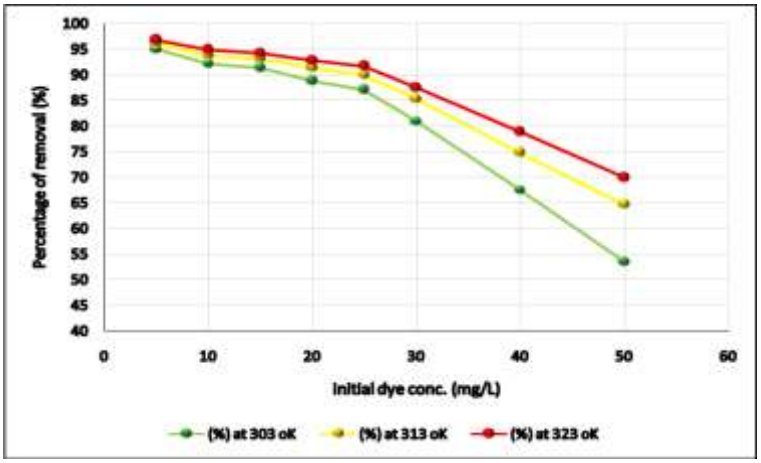

Fig. (14).Thermodynamics Study for MB dye

3.2.7. Comparative adsorption study for (AS) before and after improvement.

3.2.7.1 Effect of initial dye concentration on adsorption:

As shown from Figure (15), with fixed experimental conditions (adsorbent dose 0.1 g/100 ml; contact time 30 min; solution temperature 30^{o}C; pH 7 stirring speed 100 rpm), the maximum adsorption removal of dye by Alum sludge was 8.85% at 5 mg/L of dye conc. and the minimum adsorption removal was 0.5% at 50 mg/L of dye conc. The maximum adsorption removal of dye by composite adsorbent was 94.96 % at 5 mg/L of dye conc. and the minimum adsorption removal was 52.48 % at 50 mg/L of dye conc.

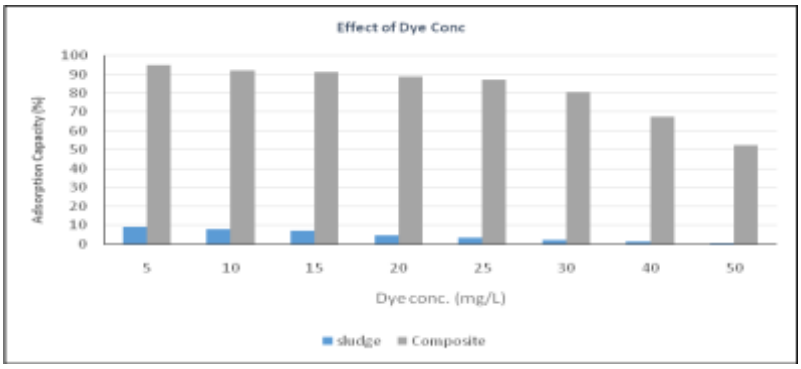

Fig. (15). Effect of initial dye concentration on Adsorption process in case of (AS) and composite.

3.2.7.2. Effect of pH on Adsorption:

From Figure (16) it was obvious with fixed experimental conditions(adsorbent dose 0.1 g/100 ml; contact time 30 min; solution temperature 30^{o}C;dye conc. of 10 mg/L and stirring speed 100 rpm),the maximum adsorption removal of dye by Alum sludge adsorbent was 8.80% at pH 7 and the minimum adsorption removal was 3.5% at pH 3. The maximum adsorption removal of dye by composite adsorbent was 90.67 % at pH 7 and the minimum adsorption removal was 53.52 % at pH 3.

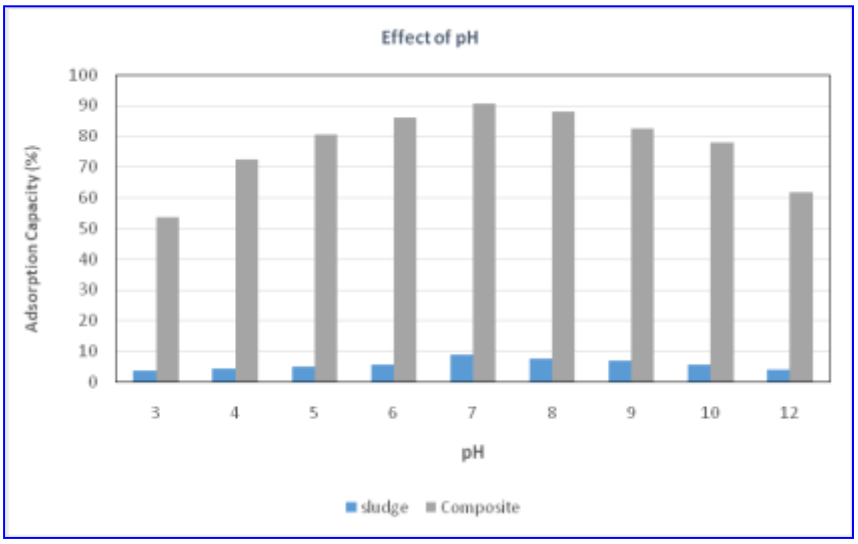

Fig. (16). Effect of pH on Adsorption process in case of (AS) and composite.

3.2.7.3. Effect of initial composite dose on dye Adsorption:

It is clear from Figure (17) that, with fixed experimental conditions (pH 7; contact time 30 min; solution temperature 30^{o}C; dye conc. of 10 mg/L and stirring speed 100 rpm), the maximum adsorption removal of dye by Alum sludge adsorbent was 12.4 % at adsorbant dose 0.2 g/100 ml and the minimum adsorption removal was 5.6% at adsorbent dose 0.05 g/100 ml. The maximum adsorption removal of dye by composite was 90.83 % at adsorbent dose about 0.1 g/100 ml and the minimum adsorption removal was 85.05 % at adsorbent dose 0.05 g/100 ml.

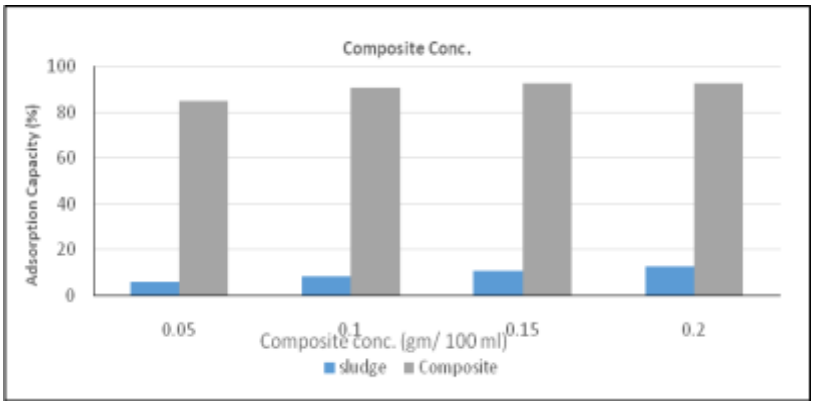

Fig. (17). Effect of initial composite dose on Adsorption process in case of (AS) and composite.

3.2.7.4. Effect of Contact Time on dye Adsorption:

From Figure (18) it was found that, with fixed experimental conditions(pH 7; 0.1 g/100 ml of adsorbent dose; solution temperature 30^{o}C; dye conc. of 10 mg/L and stirring speed 100 rpm),the maximum adsorption removal of dye by Alum sludge adsorbent was 8.88 % at contact time nearly 60 minutes. The maximum adsorption removal of dye by composite adsorbent was 92.2 % at contact time nearly 30 minutes.

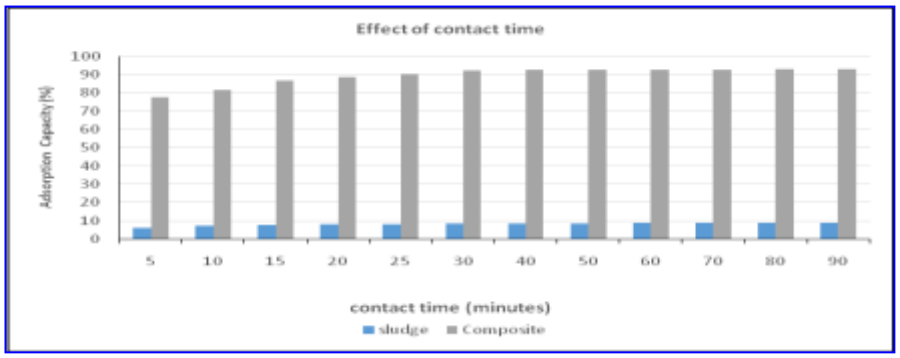

Fig. (18). Effect of contact time on adsorption process in case of (AS) and composite.

3.3. Adsorption isotherms:

Figure (19) represents the relation between C_e/q_e and C_e the variables of Langmuir adsorption isotherm. It is clear from the relationship profile that the obtained line is straight and the langmuir adsorption isotherm is well fit the adsorption process. Furthermore, the correlation coefficient of the data (R^2) is too close to unity (≈1.0) which indicates that Langmuir adsorption isotherm is well fit the adsorption process. This indicates the homogeneity of the adsorbed monolayer of the studied dye (MB) onto the composite surface and also the absence of interactions between the adsorbed dye on the composite. The value of K_L is lower than 1 which confirms that the adsorption of dye on composite is homogeneous.

It was clear from the Freundlich adsorption isotherm profile of MB dye adsorption on composite (Fig. 20) that the linear regressions of the adsorption data of the studied system were performed but the correlation coefficient of the data (R^2) is lower than the Langmuir isotherm. In addition, the obtained parameters K_F (adsorption constant) and n_f indicate that the adsorption is more homogeneous. Higher values of n_f indicates the homogeneity between the active sites and the adsorbed dye on the composite surface; while lower n_f value than 1 indicates the heterogeneity of these active sites (Li *et al.*, 2005). So the n_f value indicates the homogeneity or heterogeneity of the adsorption sites of the composite was (2.19) which means that the value is larger than 1 which indicates that for the adsorption of MB dye the active sites which attached to these dye are more homogeneous. The homogeneous of the adsorption of MB on composite indicates that the adsorption process occurred through physical adsorption on these adsorbent.

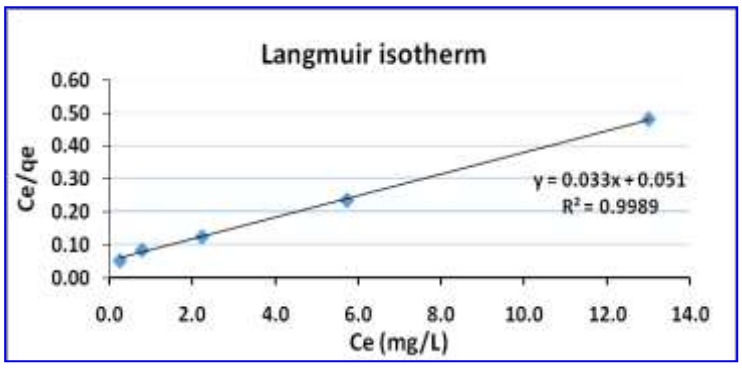

Fig. (19). Langmuir isotherm model plots for adsorption of (MB).

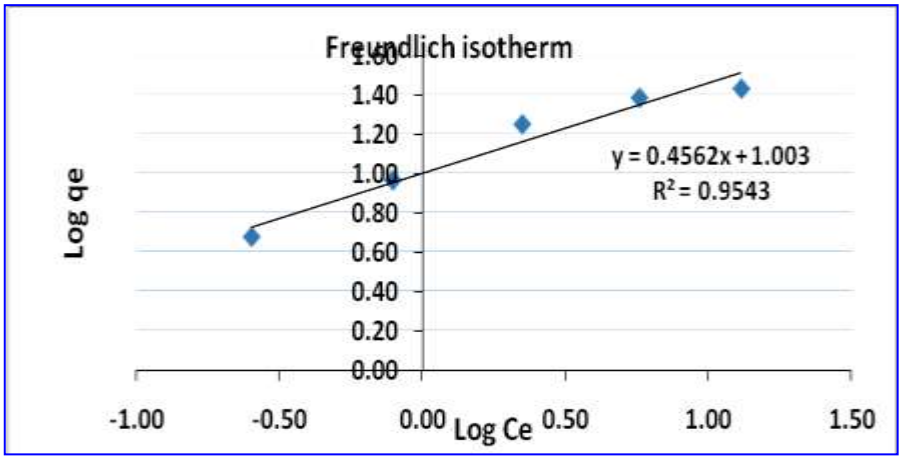

Fig. (20). Freundlich isotherm model plots for adsorption of (MB) dye.

Figure (21) represents the Temkin adsorption isotherm profile of MB dye adsorption on composite. This isotherm contains a factor that explicitly taking into the account of adsorbent–adsorbate interactions. By ignoring the extremely low and large value of concentrations, the model assumes that heat of adsorption (function of temperature) of all molecules in the layer would decrease linearly rather than logarithmic with coverage (Aharoni and Ungarish, 1977; Tempkin and Pyzhev, 1940). As implied in the equation, its derivation is characterized by a uniform distribution of binding energies (up to some maximum binding energy) was carried out by plotting the quantity sorbed (qe) against (ln Ce) where coefficients α and β are easily obtained from the slope and intercept of the linearized isotherm.

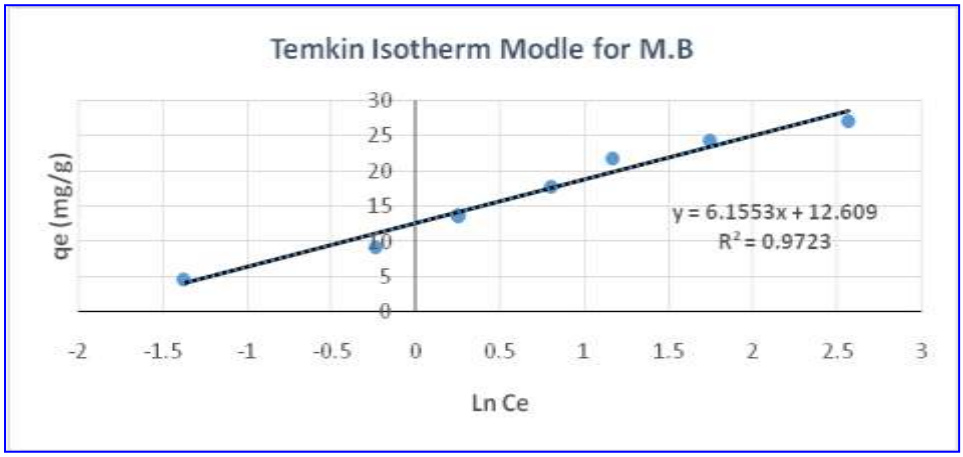

Fig. (21). Temkin isotherm model plots for adsorption of (MB) dye.

Table (3). Langmuir, Freundlich and Temkin isotherm constants for adsorption of (MB) dye.

Adsorption isotherm										
Langmuir				Freundlich			Temkin			
R^2	q_m (mg/g)	K_L	R_L	R^2	k_f	n_f	R^2	B (J/mol)	α (L/g)	b (Temkin const.) (J/mol)
0.9989	30.29	0.65	0.24	0.9543	10.07	2.19	0.9723	6.16	0.717	368.74

3.4. Adsorption kinetics

The adsorption kinetics and rate determining steps of the MB dye adsorption process onto the adsorbent can be determined and explained from the adsorption kinetic models. The most known and applicable kinetic models of heavy metal adsorption on the adsorbent are pseudo-first-order and pseudo-second-order kinetic models. The rate determining steps of the adsorption process include: diffusion control, chemical reactions and intraparticle diffusion.

1- Pseudo-first-order kinetic model:

The pseudo-first-order kinetic model suggests that the rate of sorption is proportionally dependant to the number of adsorption active sites of the adsorbents. The pseudo-first-order kinetic model of Lagergren (Pradhan *et al.*, 2005) is expressed as follows:

$\text{Ln } (qe\text{-}qt) = \text{Ln } qe - K_1 t$

where, qe and qt: the amounts of MB dye adsorbed onto the composite (mg/g) at equilibrium and at time t, respectively, and

k_1: the rate constant of pseudo-first-order kinetic model (min^{-1}).

The straight-line of the relationship between Ln (qe− qt) and t was used to establish the theoretical equilibrium adsorption concentration ($qe_{(theo)}$), rate constant of pseudo-first-order kinetic model (k_1) and correlation coefficient R^2 (Table 4). It was clear from Table (4) the large difference between $qe_{(exp)}$ and $qe_{(theo)}$ in addition to the comparatively low value of R^2 for the relation.

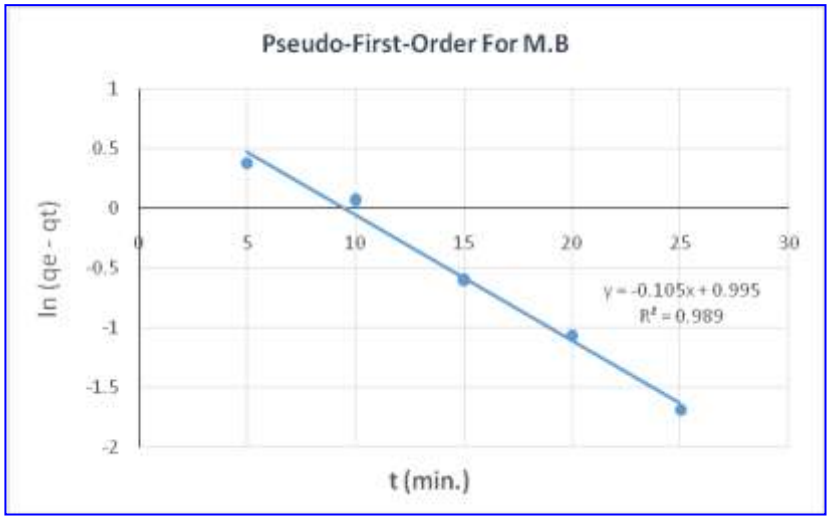

Fig. (22). Fitting of kinetic data to the pseudo-fist order kinetic model.

Table (4).The pseudo-fist order kinetic constants for adsorption of (MB) dye.

R^2	$qe_{exp.}$	$qe_{theo.}$	K1
0.9893	9.22 mg/g	-0.004108 mg/g	0.1054

Furthermore, Figure (22) showed a presence of some negative values located at longer periods of the process. The data listed in Table (4) and Figure (22) showed that the disagreement between the experimental and theoretical q_e values, which indicated the poor fit of pseudo-first-order kinetic model for the adsorption data (Ahmad *et al.*, 2016). In addition, the negative values in the kinetic model profile reveal that the kinetic model does not fit the whole range of contact time, but it is only applicable for the initial stage of the adsorption process (Unlu and Ersoz. 2006).

2- pseudo-second-order kinetic model:

To get suitable prediction for the kinetics of the adsorption process of MB dye using ASRHNMC, pseudo-second-order kinetic model was applied using its equation of state as follows: $t/q_t = 1/K_2\ q_e^2 + t/q_e$

where: q_t and q_e are the amounts of MB dye adsorbed on composite in mg/g at time t and the equilibrium, and

$k_2$is the pseudo-second order kinetic model rate constant in g/mg min.

The pseudo-second-order kinetic model (if applicable) predicts the rate determining step of the adsorption process and the bonds nature between the adsorbents and the MB dye. Figure (23) represents the variation of t/qt against time (t) of the studied system, i.e., pseudo-second-order kinetic model profile. The straight line represented the relationship is used to calculate the rate constant of the model (k_2) and correlation coefficient (R^2). The obtained data from Figure 23) were listed in Table (5).

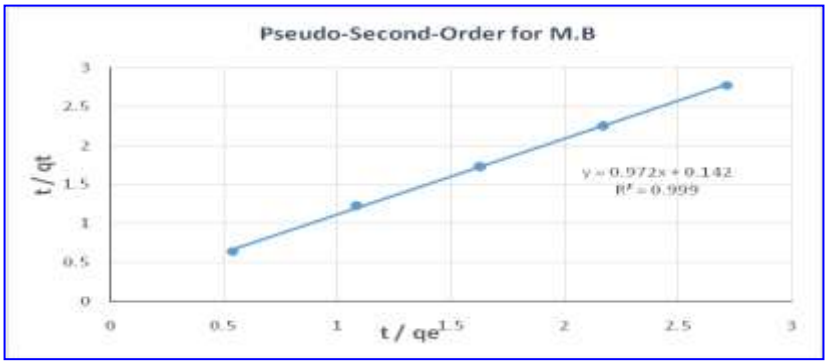

Fig. (23). Fitting of kinetic data to the pseudo-second order kinetic model.

Table (5). The pseudo-second order kinetic constants for adsorption of (MB) dye.

R^2	K2	$qe_{(exp).}$	$qe_{(theo.)}$
0.9994	0.08284	9.22	9.2201

It was clear from data in Table (5) that for the pseudo-second-order kinetic model, the correlation factors are almost equal to unity, moreover, the obtained $q_{e(theo)}$ values were in good agreement with $q_{e(exp)}$. Based on the high correlation between the obtained and measured values, it is reasonable to conclude that the pseudo-second-order kinetic model is

applicable for description of the adsorption of MB dye on the prepared composite through the whole range of process time.

Moreover, some of the adsorption process was occurred by chemisorption binding and this involves formation of chemical bonds between the composite function groups (adsorption active sites) and the MB dye via exchange or share of valence electrons (Crini, and Badot, 2008; Hasan *et al.*, 2008).

3- Intraparticle diffusion kinetic model:

Figure (24) represents the straight line plots of (q_t) vs. ($t^{1/2}$), and was used to express the rate constant of the intraparticle diffusion step (k_{int}) and the correlation coefficient (R^2). The values of the intraparticle diffusion kinetic constants for adsorption of (MB) dye are shown in Table (6).The fit line obtained is linear indicating that the intraparticle diffusion is involved in the adsorption process. The graph also indicates that the adsorption process takes place through few steps processes including a fast increasing step at the beginning, then slowing down step. The linear plot didn't pass through the origin of the graph, indicating that intraparticle diffusion is not the only rate-controlling step; other main factors, such as surface area, pore size, and volume may affect the rate of the adsorption (Kuai and Nan, 2014).

According to the analysis of R^2 values, pseudo-second-order model is the most suitable one to describe the kinetics of MB adsorption on the investigated composite This indicates that the rate-determining step of the adsorption process may be a chemical sorption one involving valence forces through sharing or exchange of electrons between adsorbent and adsorbate (Zhang *et al.*, 2016; Li *et al.*, 2015; Zhu *et al.*, 2012). In other words, the rate of the adsorption process depends upon the availability of the active adsorption sites rather than the adsorbate concentration in the bulk solution (ElShafei *et al.*, 2014). Intraparticle diffusion mechanism seems to take part in the adsorption process.

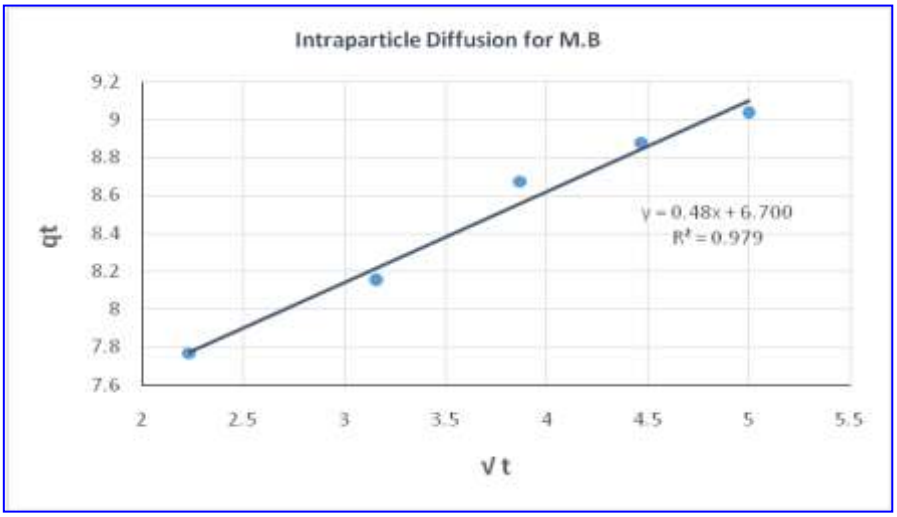

Fig. (24). Fitting of kinetic data to the intraparticle diffusion model.

Table (6). The intraparticle diffusion kinetic constants for adsorption of (MB) dye.

R^2	Ki	C intercept	Slope
0.9795	0.48	6.7007	0.48

The equation of state of the intraparticle diffusion kinetic model is expressed as follows: $q_t = k_{int}\, t^{1/2}$ where: q_t: amount of MB dye adsorbed by composite in mg/g after (t) time. k_{int}: rate constant of intraparticle diffusion step in mg/g $min^{1/2}$.

Thermodynamic parameters:

It is obvious from Figure (25 a, b) and Table (7) that MB adsorption by composite is a physisorption process (Huang *et al.*, 2011). This result agreed with that of (Shanmuga. *et al.*, 2015) who found that the adsorption of MB dye by Magnetized nanocomposite mesoporous silica is through a spontaneous, endothermic and physisorption process.

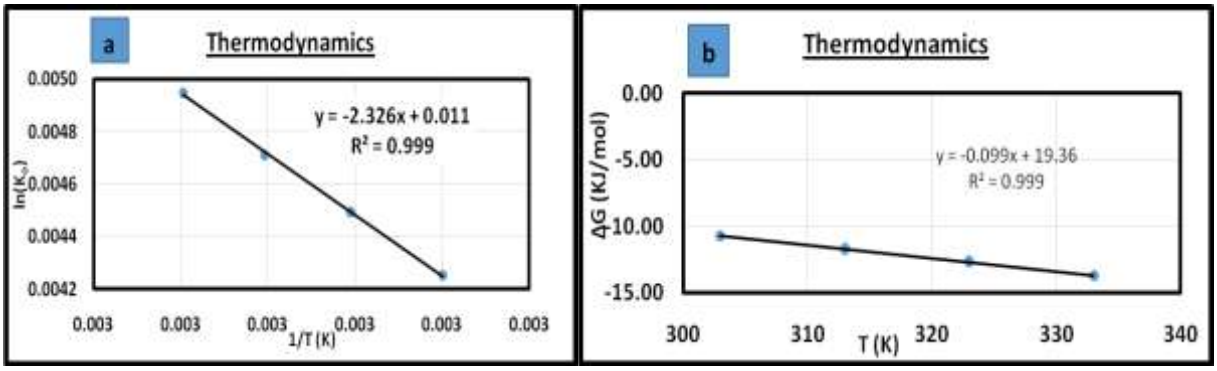

Fig. (25 a, b). Thermodynamic relations.

Table (7). Thermodynamic items for adsorption of (MB) dye by using ASRHNMC **.**

T (K)	Ka	(ΔG^o) (kJ/mol)	Slope (ΔS^o) KJ mol^{-1} K^{-1}	Intercept (ΔH^o) KJ mol^{-1}
303	**70.34**	**-10.71**	**0.10**	**19.36**
313	**89.54**	**-11.70**		
323	**111.42**	**-12.66**		
333	**141.06**	**-13.70**		

(-ΔG) mean the reaction was spontaneous. Decreasing in ΔG values means that the reaction depends on the Temp. increasing. ΔH has positive values mean the reaction was endothermic. ΔS positive values mean the adsorbent was change with Temp. increase.

Repeatability Study

A promising adsorbent should have a steady adsorption capacity in parallel experiments. The repeatability of ASRHNMC for adsorption of MB was investigated by analyzing five samples containing the same concentration of cationic dye, adsorbent dose and the same experimental conditions (pH, Temp., the same stirring rate and the same contact time). It was clear from Figure (26) that the adsorption process is nearly constant and stable with mean 92.48% $\pm$ 0.4311.

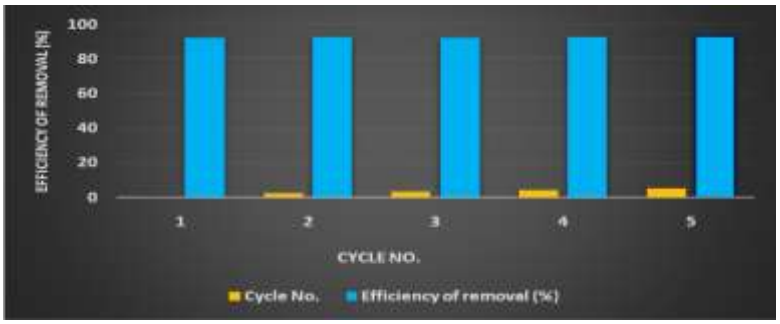

Fig. (26). Repeatability ASRHNMC for adsorption of MB dye in aqueous solutions

Regeneration Study of ASRHNMC **after (MB) dye adsorption:**

Recycling and reuse are of great importance for adsorbents in practical applications. It was obvious from Figure (27) that the adsorption rates of the adsorbent ASRHNMC for MB remained above 70% after four consecutive adsorption /desorption cycles. So it can be concluded that adsorbent has a good reusability for removing the cationic dyes in aqueous solution. However, there is some reduction in adsorption efficiency and this may be due to MB dye not being released completely from adsorption sites between cycles.

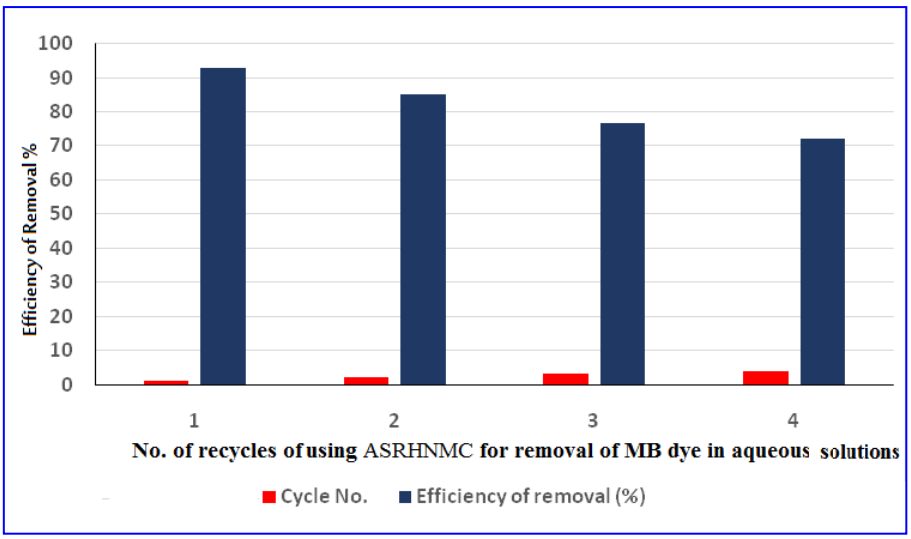

Fig.. (27). Results of recycles of using ASRHNMC to remove MB dye in aqueous solutions.

Conclusion

The Alum Sludge produced as a waste from drinking water treatment plant had been recycled to be used for removal of methylene dye in aqueous solutions by improving its characteristics through adding Rice Husk and Nano-Magnetite to form a new and novel cheap Composite (ASRHNMC). This composite has adsorption characteristics exceed Dried Alum Sludge (AS) due to the presence of high ratio Mesoporous amorphous silica and optimum ratio of Nano-magnetite which have highly adsorption characters in addition to the magnetic parameter which enable it to easily collect after adsorption process from the aqueous solution.

High adsorption removal of MB was about 92.5% on the developed adsorbent at initial dye concentration 10 mg/L, pH 7, adsorbent dosage 0.1 g/100 ml, contact time 30 minutes, solution temperature 30^{O}C and mixing rate 100 (rpm).

The adsorption data of MB dye on adsorbent fitted well with the Langmuir modeland pseudo-second order kinetic. The thermodynamic parameters were found to be thermodynamically favorable physical adsorption process.

Replacement of these unwanted wastes (Alum Sludge and Rice Husk) into recycle resources can provide alternatives solution to solve other pollution problems caused by industrial waste dyes.

REFERENCES

Agarwal, S.; Tyagi, I.; Gupta, V.K.; Ghasemi, N.; Shahivand, M. and Ghasemi, M. (2016). Kinetics, equilibrium studies and thermodynamics of methylene blue adsorption on Ephedra strobilacea saw dust and modified using phosphoric acid and zinc chloride. J. Mol. Liq., 218: 208-218.

Aharoni, C. and Ungarish, M. (1977). Kinetics of activated chemisorption. Part 2.-Theoretical models. J. Chem. Soc., Faraday Transactions 1: Physical Chemistry in Condensed Phases, 73: 456-464.

Ahmad, M.; Manzoor, K.; Venkatachalam, P. and Ikram, S. (2016). Kinetic and thermodynamic evaluation of adsorption of Cu (II) by thiosemicarbazide chitosan. Int. J. Biol. Macromolecules, 92: 910-919.

Ahn, Y.; Choi, E.J. and Kim, E.H. (2003). Superparamagnetic relaxation in cobalt ferrite nanoparticles synthesized from hydroxide carbonate precursors. Reviews on Advanced Materials Science, 5: 477-480.

Al-Fatlawi, A.H. and Neamah, M.M. (2015). Batch experiment and adsorption isotherm of phosphate removal by using drinking water treatment sludge and red mud. Int. J. Adv. Res. Sci. Engin. Technol., 2(3): 557-571.

Alyoshina, N.A. and Parfenyuk, E.V. (2013). Functionalized mesoporous silica materials for molsidomine adsorption: Thermodynamic study. J. Solid State Chem., 205: 211-216.

Besharati, N., Alizadeh, N., & Shariati, S. (2018). Removal of cationic dye methylene blue (MB) from aqueous solution by Coffee and Peanut husk Modified with Magnetite Iron Oxide Nanoparticles. Journal of the Mexican Chemical Society, 62(3).

Chungsangunsit, T.; Gheewala, S.H. and Patumsawad, S. (2009). Emission assessment of rice husk combustion for power production. World Academy of Science: Engin. Technol., 53: 1070.

Corda, N.C. and Kini, M.S. (2018). A review on adsorption of cationic dyes using activated carbon. In MATEC Web of Conferences (Vol. 144, p. 02022). EDP Sciences.

Crini, G. and Badot, P.M. (2008). Application of chitosan, a natural aminopolysaccharide, for dye removal from aqueous solutions by adsorption processes using batch studies: A review of recent literature. Progress in Polymer Science, 33(4): 399-447.

Deshmukh, P.; Bhatt, J.; Peshwe, D. and Pathak, S. (2012). Determination of silica activity index and XRD, SEM and EDS studies of amorphous SiO 2 extracted from rice Husk Ash. Transactions of the Ind. Institute of Metals, 65(1), 63-70.

Doke, S.M. and Yadav, G.D. (2014). Novelties of combustion synthesized titania ultrafiltration membrane in efficient removal of methylene blue dye from aqueous effluent. Chemosphere, 117: 760-765.

ElShafei, G.M.; ElSherbiny, I.M.; Darwish, A.S. and Philip, C.A. (2014). Silkworms' feces-based activated carbons as cheap adsorbents for removal of cadmium and methylene blue from aqueous solutions. Chem. Eng. Res. Design, 92(3): 461-470.

Fatemeh, A.; Ali, H. and Sirous, N. (2013). Surface modification of Fe3O4@SiO2 microsphere by silane coupling agent. J. In. Nano Letters, 3:23.DOI: 10.1186/2228-5326-3-23

Freundlich, H. (1907). Über die adsorption in lösungen. Zeitschrift für physikalische Chemie, 57(1): 385-470.

Fu, X.; Chen, X.; Wang, J. and Liu, J. (2011). Fabrication of carboxylic functionalized superparamagnetic mesoporous silica microspheres and their application for removal basic dye pollutants from water. Microporous and Mesoporous Materials, 139(1-3): 8-15.

Ghasemi, M.; Mashhadi, S.; Asif, M.; Tyagi, I.; Agarwal, S. and Gupta, V.K. (2016). Microwave assisted synthesis of tetraethylenepentamine functionalized activated carbon with high adsorption capacity for Malachite green dye. J. Mol. Liq., 213:317-325.

Gong, J.L.; Wang, B.; Zeng, G.M.; Yang, C.P.; Niu, C.G.; Niu, Q.Y. and Liang, Y. (2009). Removal of cationic dyes from aqueous solution using magnetic multi-wall carbon nanotube nanocomposite as adsorbent. J. Hazardous Materials, 164(2-3): 1517-1522.

Hasan, M.; Ahmad, A.L. and Hameed, B.H. (2008). Adsorption of reactive dye onto cross-linked chitosan/oil palm ash composite beads. Chem. Eng. J., 136(2-3): 164-172.

Hashemian, S.; Dehghanpor, A. and Moghahed, M. (2015). CuO. 5MnO. 5Fe2O4 nano spinels as potential sorbent for adsorption of brilliant green. J. Industrial and Engineering Chem., 24: 308-314.

Hegazy, B. E. E., Fouad, H. A., & Hassanain, A. M. (2012). Brick manufacturing from water treatment sludge and rice husk ash. Australian Journal of Basic and Applied Sciences, 6(3), 453-461.

Huang, C.H.; Chang, K.P.; Ou, H.D.; Chiang, Y.C. and Wang, C. F. (2011). Adsorption of cationic dyes onto mesoporous silica. Microporous and Mesoporous Materials, 141(1-3): 102-109.

Iara, J.F.B.; Daiane, C.; Felipe, A.L.S.; Alini, L.D.C.; Tatiana, L.A.; Carlos, A.M.; Vânia C. (2017). Characterization of silica produced from rice husk ash: Comparison of purification and processing methods. J. Materials Res., 20(Suppl. 2):512-518. DOI: http://dx.doi.org/10.1590/1980-5373-MR-2016-1043

Jurado, E.; Fernández-Serrano, M.; Nunez-Olea, J.; Luzon, G. and Lechuga, M. (2006). Simplified spectrophotometric method using methylene blue for determining anionic surfactants: Applications to the study of primary biodegradation in aerobic screening tests. Chemosphere, 65(2:, 278-285.

Khalilollah, M. and Seyed, M.M. (2019). Removing Methylene Blue from Aqueous Solutions Using Rice Husk Silica Adsorbent. Pol. J. Environ. Stud. Vol. 28, No. 4 (2019), 2281-2287

Kittappa, S.; Pichiah, S.; Kim, J. R.; Yoon, Y.; Snyder, S. A. and Jang, M. (2015). Magnetised nanocomposite mesoporous silica and its application for effective removal of methylene blue from aqueous solution. Separation and Purification Technology, 153, 67-75.

Kuai, S. and Nan, Z. (2014). Formation of sandwich structured ZnCeO. 03Fe1. 97O4@ nSiO2@ SBA-15 and adsorptive removal of methylene blue from aqueous solution. Chem. Eng. J., 244: 273-281.

Kuo, W.S. and Ho, P.H. (2001). Solar photocatalytic decolorization of methylene blue in water. Chemosphere, 45(1): 77-83.

Kurama, H. and Kurama, S.K. (2003). The effect of chemical treatment on the production of active silica from rice husk. In 18th international mining congress and exhibition of Turkey-IMCET (pp. 431-435).

Langmuir, I. (1916). The constitution and fundamental properties of solids and liquids. Part I. Solids. J. Am. Chem.. Soc., 38(11): 2221-2295.

Lee, C.I.; Yang, W.F. and Chiou, C.S. (2006). Utilization of water clarifier sludge for copper removal in a liquid fluidized-bed reactor. J. Hazardous Materials, 129(1-3): 58-63.

Li, Y.; Zhou, Y.; Nie, W.; Song, L. and Chen, P. (2015). Highly efficient methylene blue dyes removal from aqueous systems by chitosan coated magnetic mesoporous silica nanoparticles. J.Porous Materials, 22(5): 1383-1392.

Li, Y.H.; Di, Z.; Ding, J.; Wu, D.; Luan, Z. and Zhu, Y. (2005). Adsorption thermodynamic, kinetic and desorption studies of Pb2+ on carbon nanotubes. Water Res., 39(4): 605-609.

Liliana, G.; Alessandro, E. and Juan, C.M. (2013). Magnetite nanoparticles for removal of heavy metals from aqueous solutions: synthesis and characterization. J. Springer Sci., 19:465–474.

Maksum, A.; Rustandi, A.; Permana, S. and Soedarsono, J. W. (2017). Influence of roasting-quenching pretreatment on the rice husk silica prepared by calcination method. In AIP Conference Proceedings (Vol. 1823, No. 1, p. 020009). AIP Publishing LLC.

Mohamed, B.; Rachid, H.; Mohammed, K.; Mohammed, A.; Nasser, H.S.; Emad, M.M.E.; Riyad, M.E. and Adel, A. (2017). Rice husk template water treatment sludge as low cost dye and metal adsorbent. J. Egypt. J. Petrol.,26: 661–668.

Oliveira, L.C.; Rios, R.V.; Fabris, J.D.; Sapag, K.; Garg, V.K. and Lago, R.M. (2003). Clay–iron oxide magnetic composites for the adsorption of contaminants in water. Appl. Clay Sci. 22(4): 169-177.

Omar Cherkaoui, Abderrahim El Bachiri, Ahmed El Harfi. (2019). Textile finishing dyes and their impact on aquatic environs. J. Heliyon., 5: e02711

Pradhan, S.; Shukla, S. S. and Dorris, K. L. (2005). Removal of nickel from aqueous solutions using crab shells. J. Hazardous Materials, 125(1-3): 201-204.

Rafique, U.; Biplob, K.D.; Mohammad, Y.A. and Mollah, S. (2014). Characterization of Silica Coated Iron-Oxide Composites of Different Ratios. J. Int. J. Com. Mat., 2014, 4(2): 135-145.

Ramavandi, B. and Leili, M. (2015). Efficiency of shrimp shell to remove methylene blue from aqueous solutions. J. Health, 5(4): 310-325.

Rashed, M.N.; El Taher, M.E.D. and Fadlalla, S.M.M. (2016). Adsorption Kinects and Isotherms for Removal of Rhodamine B (dye) using Adsorbents prepared from drinking water treatment sludge.

Regel-Rosocka, M. and Szymanowski, J. (2005). Direct yellow and methylene blue liquid–liquid extraction with alkylene carbonates. Chemosphere, 60(8): 1151-1156.

Rhaman, M.T.; Haque, M.A.; Rouf, M.A.; Siddique, M.A.B. and Islam, M.S. (2015). Preparation and characterization of activated carbon and amorphous silica from rice husk. Bangladesh J. Sci. Industrial Res., 50(4): 263-270.

Salem, I.A. and El-Maazawi, M.S. (2000). Kinetics and mechanism of color removal of methylene blue with hydrogen peroxide catalyzed by some supported alumina surfaces. Chemosphere, 41(8): 1173-1180.

Siswoyo, E.; Mihara, Y. and Tanaka, S. (2014). Determination of key components and adsorption capacity of a low cost adsorbent based on sludge of drinking water treatment plant to adsorb cadmium ion in water. Appl. Clay Sci., 97: 146-152.

Soleha, M.Y.; Ong, K.K.; Wan, M.Z.; Wan, Y.A.; Fitrianto, M.B.; Ahmad, N.A.I; Mohd, J.O. and Teoh, C.C. (2017). Adsorption kinetics and isotherm of methylene blue by thermally treated alum-based water treatment plant sludge. Int. J.Adv. Appl. Sci., 4(12): 89-93.

Tauana, R.; Eduarda. B.; Amanda, F.; Gustavo, L.C.; Luciano, L.S.; Micheli, Z.; Josiane, M.M. and Márcio, A.F. (2019). Fe3O4@C core-shell nanoparticles as adsorbent of ionic zinc: evaluating of the adsorptive capacity. J. Materials Res., 22(suppl. 1): e20180847. DOI: http://dx.doi.org/10.1590/1980-5373-MR-2018-0847

Tempkin, M.I. and Pyzhev, V. (1940). Kinetics of ammonia synthesis on promoted iron catalyst. Acta Phys. Chim., USSR, 12: 327–356.

Tribe, N. (1974). Utilization and recycling of agricultural wastes/byproducts: A country Report.

Ünlü, N. and Ersoz, M. (2006). Adsorption characteristics of heavy metal ions onto a low cost biopolymeric sorbent from aqueous solutions. J. Hazardous Materials, 136(2): 272-280.

Vargas, A.M.; Cazetta, A.L.; Kunita, M.H.; Silva, T.L. and Almeida, V.C. (2011). Adsorption of methylene blue on activated carbon produced from flamboyant pods

(*Delonix regia*): Study of adsorption isotherms and kinetic models. Chem. Eng.. J., 168(2): 722-730.

Victor, A.R.; Villegas, J.I.; De Leo´ N.R.; Esteban, H.G. and Sergio, P.S. (2020). Lilia Angelica Hurtado Ayala and Bertha Landeros Sanchez. J. Saudi Chem. Soc., 24: 223–235.

Wang, Y.; Yu, Y.; Li, H. and Shen, C. (2016). Comparison study of phosphorus adsorption on different waste solids: fly ash, red mud and ferric–alum water treatment residues. J. Environ. Sci., 50: 79-86.

Wu, H.F.; Wang, J.P.; Duan, E.G.; Feng, Y.F.; Wan, Z.Y.; Wu, Y.X. and Lu, Y.Q. (2019). Study on the preparation of granular alum sludge adsorbent for phosphorus removal. Water Sci. Technol., 79(12): 2378-2386.

Xiao, X.; Zhang, F.; Feng, Z.; Deng, S. and Wang, Y. (2015). Adsorptive removal and kinetics of methylene blue from aqueous solution using NiO/MCM-41 composite. Physica E: Low-dimensional Systems and Nanostructures, 65: 4-12.

Yalcin, N. and Sevinc, V. (2001). Studies on silica obtained from rice husk. Ceramics Int. J., 27: 219-24.

Yusuff, S.M., Ong, K. K., Yunus, W. M. Z. W., Fitrianto, A., & Ahmad, M. B. (2017). Removal of methylene blue from aqueous solutions using alum sludge: sorption optimization by response surface methodology. J. Fundamental Appl. Sci., 9(3S): 532-545.

Yusuff, S.M.; Khim, O.K.; Yunus, W.M.Z.W.; Fitrianto, A.; Ahmad, M.B.; Ibrahim, N.A. and Chuang, T.C. (2017). Adsorption kinetics and isotherm of methylene blue by thermally treated alum-based water treatment plant sludge. Int. Adv. Appl. Sci., 4(12): 89-93.

Zhang, J.; Lin, S.; Han, M.; Su, Q.; Xia, L. and Hui, Z. (2020). Adsorption properties of magnetic magnetite nanoparticle for coexistent Cr (VI) and Cu (II) in mixed solution. Water, 12(2): 446.

Zhang, Y.; Lin, X.; Zhou, Q. and Luo, X. (2016). Fluoride adsorption from aqueous solution by magnetic core-shell Fe3O4@ alginate-La particles fabricated via electro-coextrusion. Appl. Surface Sci., 389: 34-45.

Zhao, M.; Tang, Z. and Liu, P. (2008). Removal of methylene blue from aqueous solution with silica nano-sheets derived from vermiculite. J. Hazardous Materials, 158(1): 43-51.

Zhou, Y.F.; Haynes, R.J. and Popov, V. (2010). Water treatment sludge can be used as an adsorbent for heavy metals in wastewater streams. Waste Management and the Environment, 140: 379-389.

Zhu, H.Y.; Fu, Y.Q.; Jiang, R.; Yao, J.; Xiao, L. and Zeng, G.M. (2012). Novel magnetic chitosan/poly (vinyl alcohol) hydrogel beads: preparation, characterization and application for adsorption of dye from aqueous solution. Bioresource Technol., 105: 24-30.

Improvement and characterization of alum sludge by nano-iron oxide and rice husk for removal of methylene blue dye from aqueous solution.

تحسين وتوصيف حمأة الشبة بأكسيد الحديد النانوي وقشر الأرز لإزالة صبغة الميثيلين الزرقاء من المحلول المائي.

تامر طارق السيد محمد الطوخي[1] ، محمد عبد الحي أحمد إسماعيل[2] ، مي إبراهيم الجمال[3] ، محمود سالم ابراهيم[3]

1 - قطاع المعامل والبحوث- شركة مياه الشرب بالقاهرة الكبرى- القاهرة- مصر.

2 - قسم الكيمياء- كلية العلوم - جامعة عين شمس - مصر.

3 - قسم العلوم البيئية – كلية العلوم – جامعة دمياط – مصر.

المستخلص

في هذه الدراسة ، تم تحسين خصائص امتصاص نفايات الشبة (AS) من محطة معالجة المياه في روض الفرج عن طريق المعالجة بقشر الأرز الحمضي (RH) والنانو-ماغنتيت (NM) لتكوين مركب النانو (Magnetite ASRHNMC). اكتسب هذا المركب خصائص جديدة لمساحة السطح الكبيرة ، والبنية المسامية والخصائص المغناطيسية ، وقد تم استخدامه كمركب منخفض التكلفة لإزالة الميثيلين الأزرق (MB) كصبغة كاتيونية من محلول مائي. تم توصيف كلا من حمأة الشبة قبل المعالجة وبعد معالجتها وهي في صورة المركب الجديد (ASRHNMC) من خلال الاجهزة المختلفة مثل جهاز حيود الأشعة السينية، ميكروسكوب المسح الإلكتروني، الميكروسكوب الالكتروني الناقل، جهاز مقياس الطيف بالأشعة تحت الجمراء وغيرها للتعرف على التغير في تركيب الشبة قبل وبعد المعالجة. تم مقارنة قدرة حمأة الشبة على ادمصاص صبغة الميثيلين الزرقاء من الماء قبل وبعد معالجتها لقياس مدى التغير في قدرتها الإدمصاصية بعد المعالجة. النتائج اثبتت القدرة الكبيرة للمركب المغناطيسي النانوي الناتج عن تحسين خواص حمأة الشبة في إدمصاص صبغة الميثيلين الزرقاء وانه له القدرة على التنشيط وإعادة إستخدامه أكثر من مرة وهذا يعني انه رخيص التكلفة بجانب قدرتة الإدمصاصية الكبيرة.